Received: 18 December 2019 | Revised: 9 March 2020 | Accepted: 9 April 2020

DOI: 10.1002/hipo.23212

WILEY

RESEARCH ARTICLE

Frequency- and state-dependent effects of hippocampal neural disinhibition on hippocampal local field potential oscillations in anesthetized rats

Miriam Gwilt | Markus Bauer | Tobias Bast

School of Psychology and Neuroscience, University of Nottingham, Nottingham, UK

Correspondence
Miriam Gwilt, Markus Bauer and Tobias Bast, School of Psychology and Neuroscience, University of Nottingham, Nottingham, NG7 2RD, UK.
Email: miriam.gwilt@nottingham.ac.uk (M. G.), markus.bauer@nottingham.ac.uk (M. B.) and tobias.bast@nottingham.ac.uk (T. B.)

Funding information
Biotechnology and Biological Sciences Research Council, Grant/Award Number: iCASE award; Boehringer Ingelheim; University of Nottingham

Abstract

Reduced inhibitory GABA function, so-called neural disinhibition, has been implicated in cognitive disorders, including schizophrenia and age-related cognitive decline. We previously showed in rats that hippocampal disinhibition by local microinfusion of the GABA-A receptor antagonist picrotoxin disrupted memory and attention and enhanced hippocampal multi-unit burst firing recorded around the infusion site under isoflurane anesthesia. Here, we analyzed the hippocampal local field potential (LFP) recorded alongside the multi-unit data. We predicted frequency-specific LFP changes, based on previous studies implicating GABA in hippocampal oscillations, with the weight of evidence suggesting that disinhibition would facilitate theta and disrupt gamma oscillations. Using a new semi-automated method based on the kurtosis of the LFP peak-amplitude distribution as well as on amplitude envelope thresholding, we separated three distinct hippocampal LFP states under isoflurane anesthesia: "burst" and "suppression" states—high-amplitude LFP spike bursts and the interspersed low-amplitudeperiods—and a medium-amplitude "continuous" state. The burst state showed greater overall power than suppression and continuous states and higher relative delta/theta power, but lower relative beta/gamma power. The burst state also showed reduced functional connectivity across the hippocampal recording area, especially around theta and beta frequencies. Overall neuronal firing was higher in the burst than the other two states, whereas the proportion of burst firing was higher in burst and continuous states than the suppression state. Disinhibition caused state- and frequency-dependent LFP changes, tending to increase power at lower frequencies (<20 Hz), but to decrease power and connectivity at higher frequencies (>20 Hz) in burst and suppression states. The disinhibition-induced enhancement of multi-unit bursting was also state-dependent, tending to be more pronounced in burst and suppression states than the continuous state. Overall, we characterized three distinct hippocampal LFP states in isoflurane-anesthetized rats.

Markus Bauer and Tobias Bast contributed equally to the study.

Disinhibition changed hippocampal LFP oscillations in a state- and frequency-dependent way. Moreover, the disinhibition-induced enhancement of multi-unit bursting was also LFP state-dependent.

KEYWORDS
anesthesia, disinhibition, GABA, hippocampus, LFP, oscillations, picrotoxin

1 | INTRODUCTION

Subconvulsive neural disinhibition, that is, reduced inhibitory GABA function, within the hippocampus has been implicated in important neuropsychiatric disorders, including schizophrenia and age-related cognitive decline, and in the cognitive impairments characterizing these disorders (Bast, Pezze, & McGarrity, 2017; Benes & Berretta, 2001; Heckers & Konradi, 2015; McGarrity, Mason, Fone, Pezze, & Bast, 2017; Nava-Mesa, Jiménez-Díaz, Yajeya, & Navarro-Lopez, 2014; Palop & Mucke, 2016; Stanley, Fadel, & Mott, 2012; Thomé, Gray, Erickson, Lipa, & Barnes, 2016). In a recent study (McGarrity et al., 2017), we pharmacologically disinhibited the temporal (also known as ventral) to intermediate hippocampus in rats by acute local microinfusion of the GABA-A receptor antagonist picrotoxin. Such hippocampal disinhibition caused clinically relevant cognitive impairments, including in hippocampal memory function and in attentional performance that relies on prefrontal–striatal mechanisms, consistent with the idea that hippocampal disinhibition disrupts both hippocampal processing and processing in hippocampal projection sites (Bast et al., 2017). In addition, electrophysiological recordings around the infusion site under isoflurane anesthesia showed that disinhibition enhanced burst firing of hippocampal neurons, as reflected by multi-unit data. The purpose of this article is to report the analysis of the impact of disinhibition on the hippocampal local field potential (LFP), which we recorded alongside the multi-unit data.

Brain rhythms or oscillations, that is, synchronized changes in the activity of many neurons, as revealed by LFP recordings have been suggested to be important for cognitive processing, including memory, because they bind neurons into functional assemblies (Buzsáki & Draguhn, 2004; Colgin, 2016). Alterations in brain rhythms have been reported in many neuropsychiatric disorders and have been suggested to arise partly from GABA dysfunction (Uhlhaas & Singer, 2006, 2010). Two prominent, widely studied hippocampal LFP rhythms are the theta and gamma rhythms. In the rat hippocampus, theta ranges from 4 to 12 Hz, whereas gamma oscillations range from 25 to 100 Hz, including "slow" or "low" gamma from 25 to 55 Hz (also known as beta rhythms) and "fast" or "high" gamma from 60 to 100 Hz (Colgin, 2016; Colgin et al., 2009). Substantial evidence suggests that theta and gamma LFP rhythms depend on hippocampal GABAergic inhibition; this evidence leads to the hypotheses underlying our study of the LFP changes caused by hippocampal disinhibition and will be considered in the following paragraphs. Another prominent hippocampal rhythm, sharp-wave ripples (110–250 Hz ripples superimposed on 0.01–3 Hz sharp waves; Colgin, 2016), will not be considered further in this article, because ripples are not expressed under volatile anesthetics (Ylinen et al., 1995), and the frequency range of our LFP recordings (0.7–170 Hz) did not encompass the full range of sharp waves and ripples.

Substantial evidence suggests that hippocampal disinhibition would facilitate hippocampal theta power. Septal projections to the hippocampus, including excitatory cholinergic projections and GABAergic projections, which disinhibit the hippocampus by innervating hippocampal inhibitory GABA interneurons (Borhegyi, Varga, Szilagyi, Fabo, & Freund, 2004; Freund & Antal, 1988; Hangya, Borhegyi, Szilágyi, Freund, & Varga, 2009; Tóth, Freund, & Miles, 1997), are thought to be a main theta driver (Colgin, 2016). In line with this, septal inactivation reliably abolishes hippocampal theta in freely moving rats (Brandon et al., 2011; Koenig, Linder, Leutgeb, & Leutgeb, 2011), and, in urethane-anesthetized rats with septal inactivation, hippocampal theta could be reinstated by cholinergic stimulation or disinhibition (with the GABA-A receptor antagonist bicuculline) of the hippocampus (Smythe, Colom, & Bland, 1992). Moreover, cholinergic stimulation of rat hippocampal slices by carbachol reliably induces theta in vitro, and pharmacological disinhibition by GABA-A receptor antagonists has been reported to enhance the amplitude of such cholinergically induced theta oscillations (Golebiewski, Eckersdorf, & Konopacki, 1996; Konopacki, Gołębiewski, Eckersdorf, Błaszczyk, & Grabowski, 1997; Kowalczyk, Bocian, & Konopacki, 2013). In line with such theta-enhancing effects of hippocampal disinhibition, hippocampal inhibition with the GABA-A receptor agonist muscimol disrupted cholinergically induced theta in the rat hippocampus in vitro (Golebiewski et al., 1996) and in vivo (Smythe et al., 1992). These findings thus support an inverse relationship between hippocampal GABA function and theta amplitude (Kowalczyk et al., 2013).

However, there is also evidence that some types and properties of hippocampal theta are positively modulated by GABA function and disrupted by hippocampal disinhibition. Genetic ablation of synaptic inhibition of parvalbumin-positive GABAergic interneurons disrupted hippocampal theta in freely moving mice (Wulff et al., 2009). GABA-A receptor antagonists reduced the power of theta induced by septal activation in an in vitro septo-hippocampal preparation from rats (Goutagny, Manseau, Jackson, Danik, & Williams, 2008), and of nicotine-induced(Lu & Henderson, 2010) and electrically induced (Heynen, Sainsbury, & Bilkey, 1993) theta in rat hippocampal slices, and decreased frequency and coherence (connectivity) of carbachol-induced theta between the entorhinal cortex and subiculum in vitro (Levesque, Cataldi, Chen, Hamidi, & Avoli, 2017). Moreover,

optogenetic activation of parvalbumin-positive GABAergic hippocampal interneurons strengthened, whereas silencing of these neurons disrupted, theta in an in vitro preparation of the mouse hippocampus with intact intrinsic but severed extrinsic connectivity, suggesting that GABAergic inhibition by parvalbumin neurons supports intrinsically generated theta (Amilhon et al., 2015). Finally, genetic knock-out of the GABA-A receptor subunit β_3 decreased power, frequency, and regularity of hippocampal theta and theta cross-correlation between

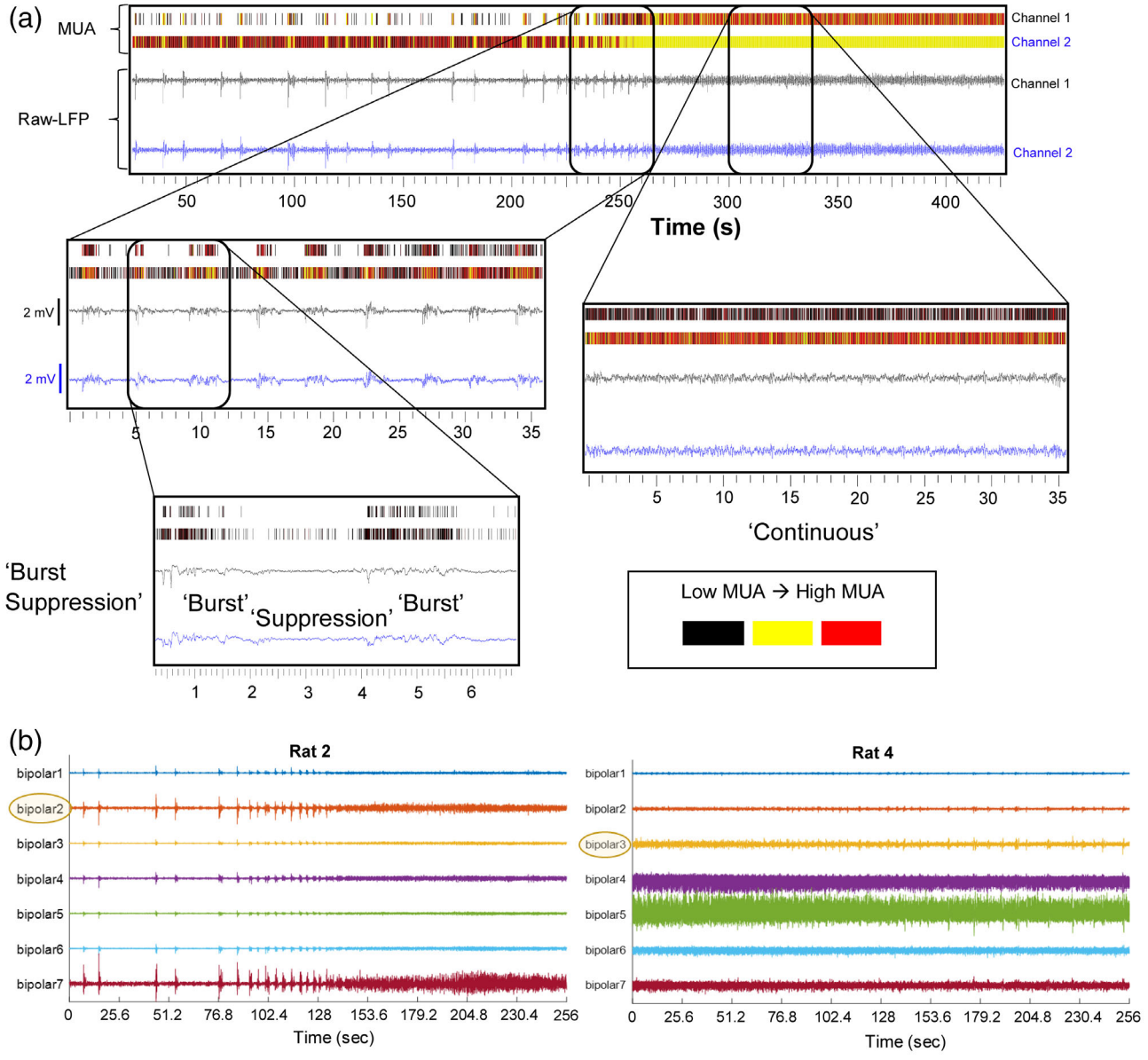

FIGURE 1 Three distinct local field potential (LFP) states in the rat hippocampus under isoflurane anesthesia. For illustration purposes, example raw traces are shown to familiarize the reader with the manifestation of the different LFP states. (a) The top panel shows two 400-s long LFP traces, with corresponding multi-unit activity (MUA), recorded simultaneously from the temporal to intermediate hippocampus under isoflurane anesthesia. They illustrate the transition from the burst-suppression state (left), comprising burst and suppression states, to the continuous state (right). The middle panel shows the 40-s sections indicated in the top panel with an expanded time line. The bottom panel depicts a 7-s period of the burst-suppression state with an expanded time line, showing the LFP signal during burst and suppression states in higher detail. The three distinct LFP states also differ with respect to multi-unit spiking, particularly MUA tends to be higher during the burst than in the suppression state (mind the color "scale," showing three distinct levels of MUA [besides zero which is transparent]—corresponding to different MUA frequencies; exported from Neuroexplorer v4). (b) The two plots show the LFP traces recorded from the montage of seven bipolar channels in two different rats to give a more representative impression of the distinctiveness of the states that differs greatly between different animals and, sometimes, electrodes. Bipolar Channel 2 of Rat 2 was selected as the "LFP state-defining" channel here because of very clear visual separation of the three states based on the amplitude differences (these are the data magnified in [a]). By contrast, in Rat 4, the three LFP states are visually less clearly separated. Channel 3 was selected as the "LFP state-defining" channel for this rat because, although it has smaller overall amplitudes than other channels, the three different states are visually more clearly separated, especially compared to Channels 4–7 [Color figure can be viewed at wileyonlinelibrary.com]

different hippocampal subfields in freely moving mice (Hentschke et al., 2009).

There is also substantial evidence linking hippocampal gamma oscillations to inhibitory GABAergic hippocampal interneurons (Colgin, 2016). In rodents, firing of hippocampal interneurons is phase-locked to spontaneous hippocampal gamma oscillations (Belluscio, Mizuseki, Schmidt, Kempter, & Buzsaki, 2012; Mann, Suckling, Hajos, Greenfield, & Paulsen, 2005; Tiesinga, Fellous, José, & Sejnowski, 2001; Traub et al., 2000; Tukker, Fuentealba, Hartwich, Somogyi, & Klausberger, 2007), and intracellularly recorded inhibitory postsynaptic potentials of pyramidal cells, recorded in vivo, are reflected in gamma oscillations (Penttonen, Kamondi, Acsady, & Buzsaki, 1998; Soltesz & Deschenes, 1993). This indicates that hippocampal gamma is generated by hippocampal GABA interneurons (Colgin, 2016). Consistent with this, GABA-A receptor antagonists have been shown to disrupt different types of experimentally induced gamma oscillations in hippocampal slices, with the magnitude of this effect depending on the hippocampal subfield (Bartos, Vida, & Jonas, 2007; Fisahn et al., 2004; Traub, Bibbig, LeBeau, Buhl, & Whittington, 2004; Whittington, Traub, Kopell, Ermentrout, & Buhl, 2000).

Overall, the above review of GABAergic mechanisms of hippocampal theta and gamma oscillations leads to the hypothesis that pharmacological hippocampal disinhibition will cause frequency-dependent changes in LFP oscillations, with the weight of evidence suggesting that gamma amplitude may be reduced, whereas theta amplitude may be enhanced. However, there is also evidence suggesting that some features of the theta rhythm, including its coherence across the hippocampus, may be disrupted.

When analyzing LFP recordings from anesthetized rodents, it is important to consider that, under anesthesia, many brain regions, including the hippocampus, show different LFP states characterized by distinct LFP patterns which can alternate (Clement et al., 2008; Kenny, Westover, Ching, Brown, & Solt, 2014; Land, Engler, Kral, & Engel, 2012; Lustig, Wang, & Pastalkova, 2016; Wolansky, Clement, Peters, Palczak, & Dickson, 2006) (for an example of our hippocampal recordings, see Figure 1a). One key LFP state observed with many anesthetics, including isoflurane, is the burst-suppression state, which can be further subdivided into a "burst" state, characterized by LFP "bursts" (i.e., high-amplitude LFP deflections), which alternates with a "suppression" state, characterized by low-amplitude LFP signal (Note: the burst-suppression state is often, or even typically, considered as one state, without further subdivision in two distinct states, although visual inspection of the LFP trace clearly suggests distinct properties of the burst and suppression components; our quantitative analysis reported in this article also revealed distinct properties of these two states). A third LFP state is characterized by a more "continuous" LFP pattern with continuous LFP activity of lower amplitude than during LFP bursts. The balance between the burst suppression and continuous states changes with anaesthetic depth, with burst-suppression tending to become more dominant, the deeper the anesthesia (Land et al., 2012; Lustig et al., 2016). To analyze the impact of neuropharmacological manipulations, including hippocampal disinhibition, on LFP oscillations under anesthesia, it is important to separate these different LFP states for two main reasons. First, the large-amplitude LFP signals characterizing the burst state reflect major non-stationarities in the otherwise low-amplitude signals and may thus dominate the power spectral analysis, occluding frequency components that may be more characteristic of the other LFP states. Second, given the distinct characteristics of LFP patterns in different LFP states, neuropharmacological mechanisms underlying oscillatory activity may be LFP-state dependent.

In the present study, we aimed to characterize the effect of hippocampal disinhibition, by picrotoxin infusions into the temporal to intermediate hippocampus, on hippocampal neural oscillations around the infusion site using the LFP data recorded by McGarrity et al. (2017). First, we developed an objective, semi-automated method to separate the three distinct LFP states described above (the continuous LFP state from the burst-suppression state, and, within the latter, the burst from the suppression state; and compared several properties of these states (frequency-specific power and connectivity, and multi-unit parameters). Second, we examined the impact of picrotoxin on hippocampal LFP properties (frequency-specific power and connectivity) in the three distinct LFP states. Third, we examined if the disinhibition-induced enhancement of multi-unit burst firing reported previously (McGarrity et al., 2017) is dependent on the LFP state.

2 | METHODS

2.1 | LFP and multi-unit data recording and preprocessing

Analysis was carried out on the hippocampal LFP and multi-unit data collected in our previous study (McGarrity et al., 2017). The recordings were carried out in accordance with the Animals (Scientific Procedures) Act 1986, and full details concerning the rats used for the recordings, housing conditions, surgical and recording procedures, and equipment can be found in our previous study (McGarrity et al., 2017). In brief, LFP and multi-unit data were recorded simultaneously in isoflurane-anesthetized male adult (2–3 months) Lister-hooded rats, using a custom-made assembly of a 33-gauge stainless steel infusion cannula and an eight-electrode (microwire) recording array that was implanted into the hippocampus (Figure 2a, top right). The cannula tip, through which saline or picrotoxin solution could be injected, touched the electrodes and was positioned about 0.5 mm above the tips of the central electrodes. The assembly was stereotactically implanted into the right hippocampus, such that the eight-electrode array was arranged perpendicular to the brain midline and anterior to the infusion cannula, with the cannula tip aimed at coordinates in the right temporal (also known as ventral) to intermediate hippocampus (5.2 mm posterior to bregma, 4.8 mm lateral from midline, and 6.5 mm ventral from dura). The eight-electrode array spread approximately 2 mm, in the mediolateral direction (Figure 2a, top left). The extracellular signal recorded by the electrodes was band-pass filtered into LFP (0.7 and 170 Hz) and multi-unit (250 Hz–8 kHz) data, which were recorded for a 30-min baseline

period and a 60-min period following infusion (over about 1 min) of either 0.5 μl saline (n = 7 rats) or 150 ng/0.5 μl picrotoxin (n = 6 rats) in a between-subjects design. Isoflurane levels were kept at a relatively stable level (1–3% depending on the rat) over the entire recording period, such that the breathing rate was kept around 50 breaths per minute and the pedal reflex was absent. All data were collected continuously and averaged in 5-min bins, that is, six pre-infusion (baseline) and 12 post-infusion5-min bins. Although the picrotoxin group in the original study included eight rats (McGarrity et al., 2017), only six could be included in the present analysis, because one of the data sets could not be read into MATLAB for analysis and another data set was recorded using a bundle array and, therefore, could not be combined with the rest of the data for LFP analysis.

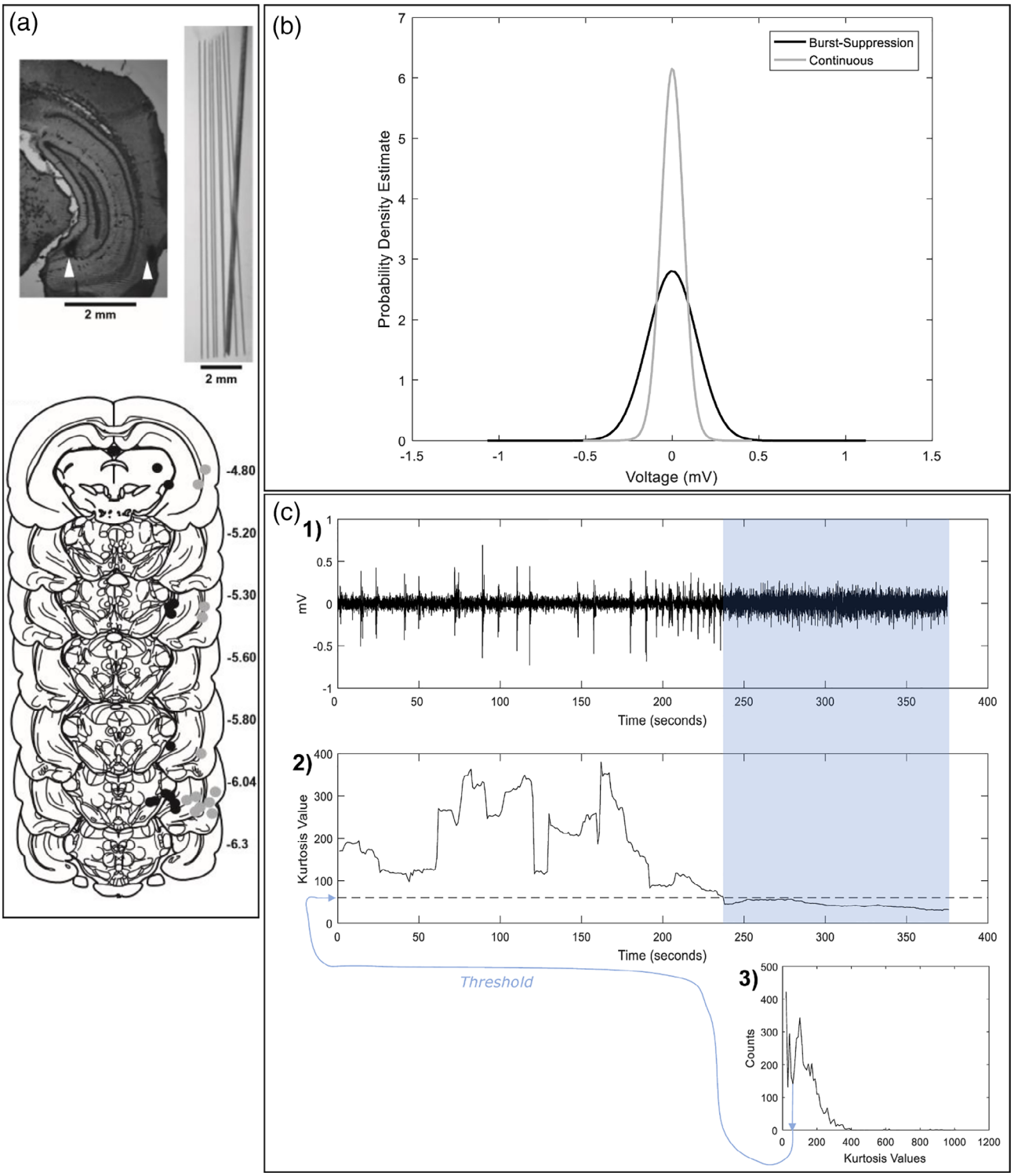

FIGURE 2 Legend on next page.

All data were processed in MATLAB (R2016a) (The MathWorks, Inc.) using the FieldTrip toolbox (Oostenveld, Fries, Maris, & Schoffelen, 2011). To reduce noise, far-field effects, and shared signal from all the electrode recordings, a montage of seven bipolar channels was digitally created using a pairwise bipolar subtraction (Land et al., 2012) of the eight original electrodes. Data were then preprocessed in FieldTrip by re-referencing with a common reference over all bipolar channels (except for the functional connectivity analysis) to remove any remaining linear gradient affecting all bipolar pairs, DC offset removal for each episode, and a band-stop filter between 49.5 and 50.5 Hz to remove the electric line noise. The most medial and/or the most lateral electrodes of the 2-mmeight-electrode recording array were located outside of the hippocampus (typically 1–3 electrodes per rat; Figure 2a, bottom), and our previous multi-unit analysis revealed that hippocampal picrotoxin infusion did not affect any of the multi-unit parameters analyzed from these electrodes (consistent with the densely packed fiber bundles surrounding the hippocampus) (McGarrity et al., 2017). If both of the electrodes used to calculate a synthetic bipolar electrode were outside the hippocampus, that particular bipolar channel was removed, otherwise it was included in the analysis. As bipolar subtraction was not appropriate for multi-unit activity (MUA), in order to match the seven bipolar channels used for the LFP analysis, electrodes 2–8 were selected and matched to their corresponding bipolar channel (i.e., electrode 2 to bipolar 1, electrode 3 to bipolar 2, etc.). Electrodes 2–8 were selected in place of 1 to 7 because in most cases electrode 1 (the most medial) sat outside the hippocampus and had to be excluded anyway.

2.2 | Semi-automated separation of LFP states

The hippocampal LFP recordings under isoflurane anesthesia clearly showed the three distinct LFP states outlined in Section 1, including a burst, suppression, and continuous state (Figure 1a). The simultaneously recorded MUA also appeared to vary depending on the LFP state, with the burst state tending to show a higher multi-unit firing than the suppression state, and the continuous state characterized by continuous firing at a similar rate to that in the burst state. Our semi-automated separation strategy was to start by separating the combined burst-suppression state from the continuous state and then to separate the burst from the suppression state.

Simple thresholding based on continuous amplitude/power measures did, with our data, not result reliably in state separation that corresponded to the states that would be assigned by visual inspection (although thresholding worked for the example LFP traces in Figure 1a, it did not reliably separate the LFP states when these showed less pronounced differences; for example, see Figure 1b, right). Therefore, we used a higher order moment (kurtosis) of the distribution of the peak amplitude values—rather than the mere amplitude of the continuous signal (see below). To separate the three states, for each rat the channel with the most marked difference between LFP states based on visual inspection of the raw LFP traces, the "LFP state-defining" channel, was selected (for example, see Figure 1b). For this LFP state-defining channel, the peaks and troughs of the LFP trace were identified (undifferentiated over baseline and post-infusion periods) by identifying the sign change of the first derivative. The distribution of these peaks and troughs identified from the signchange turned out to be unimodal (Figure 2b), and thus not enabling a clear separation into discrete states. In contrast, a measure of the kurtosis ("tailedness") of the amplitude distribution of those peaks and troughs separated the burst-suppression and continuous states. The kurtosis was calculated for a 10-s sliding window with a 1-s step size (the raw signal and the estimates of kurtosis are plotted in Figure 2c, Panels 1 and 2, respectively). A histogram of kurtosis values (a total of 4,391) was plotted in 100 bins (Figure 2c, Panel 3), and the most distinct local minimum (the first or second) separating peaks in the multimodal distribution was selected as threshold to separate the combined burst-suppression states from the continuous state (Figure 2c, arrow). If kurtosis values exceeded this threshold, the corresponding time points were marked as being in the burst-suppression state, whereas time points with subthreshold values were marked as in the continuous state (Figure 2c, shaded area). These labels were then applied to the samples of every channel from the same rat.

FIGURE 2 Hippocampal recordings and separation of hippocampal local field potential (LFP) states. (a) *Placement of the infusion-recording array within the temporal to intermediate hippocampus*. The top pictures show, right, the eight-electrode array with the attached infusion cannula and, left, an example coronal section through the hippocampus, with the placements of the most medial and most lateral electrodes indicated by the white arrow heads. The array was arranged perpendicular to the midline of the brain, with the infusion cannula located just posterior to the center of the array. In the bottom, the most medial (black dots) and most lateral (grey dots) electrode placements are indicated for all rats included in the analysis on drawings of coronal brain sections taken from the atlas by (Paxinos & Watson, 1998). Note that the most medial and/or the most lateral electrodes of the 2-mmeight-electrode recording array were located outside the hippocampus (typically one to three electrodes per rat), and data from these electrodes were excluded from the analysis. (b) *The distribution of amplitude of peaks and troughs in the burst-suppression state and the continuous state differ in kurtosis, but not modality*. A histogram was calculated for the identified peak and trough amplitudes based on visually identified 100-s segments belonging to the combined burst-suppression or the continuous state, from the 400-s trace shown in Figure 1. Both states show a unimodal amplitude distribution, but the distribution of the burst-suppression state shows a higher kurtosis (tailedness). (c) *Semiautomatic separation of burst-suppression and continuous LFP states, using the kurtosis values of the distribution of the peak and trough amplitudes of the LFP trace*. (1) 400-s LFP trace, clearly showing separate burst-suppression (white background) and continuous states (shaded) (same 400-s trace as shown in Figure 1a). (2) The time course of the kurtosis values of the 400-s LFP trace, calculated using a 10-s long, 1-s sliding window. (3) Histogram of the distribution of kurtosis values over baseline and post-infusion data (i.e., the whole recording period, not only the 400-s period presented in [1] and [2]). The arrow from (3) to (2) represents, in this case, the second minimum in the histogram (3), which corresponds to the kurtosis threshold value (stippled line in 2) that separates burst-suppression from the continuous state.
Figure 2a is adapted from figure 5A in McGarrity et al. (2017) [Color figure can be viewed at wileyonlinelibrary.com]

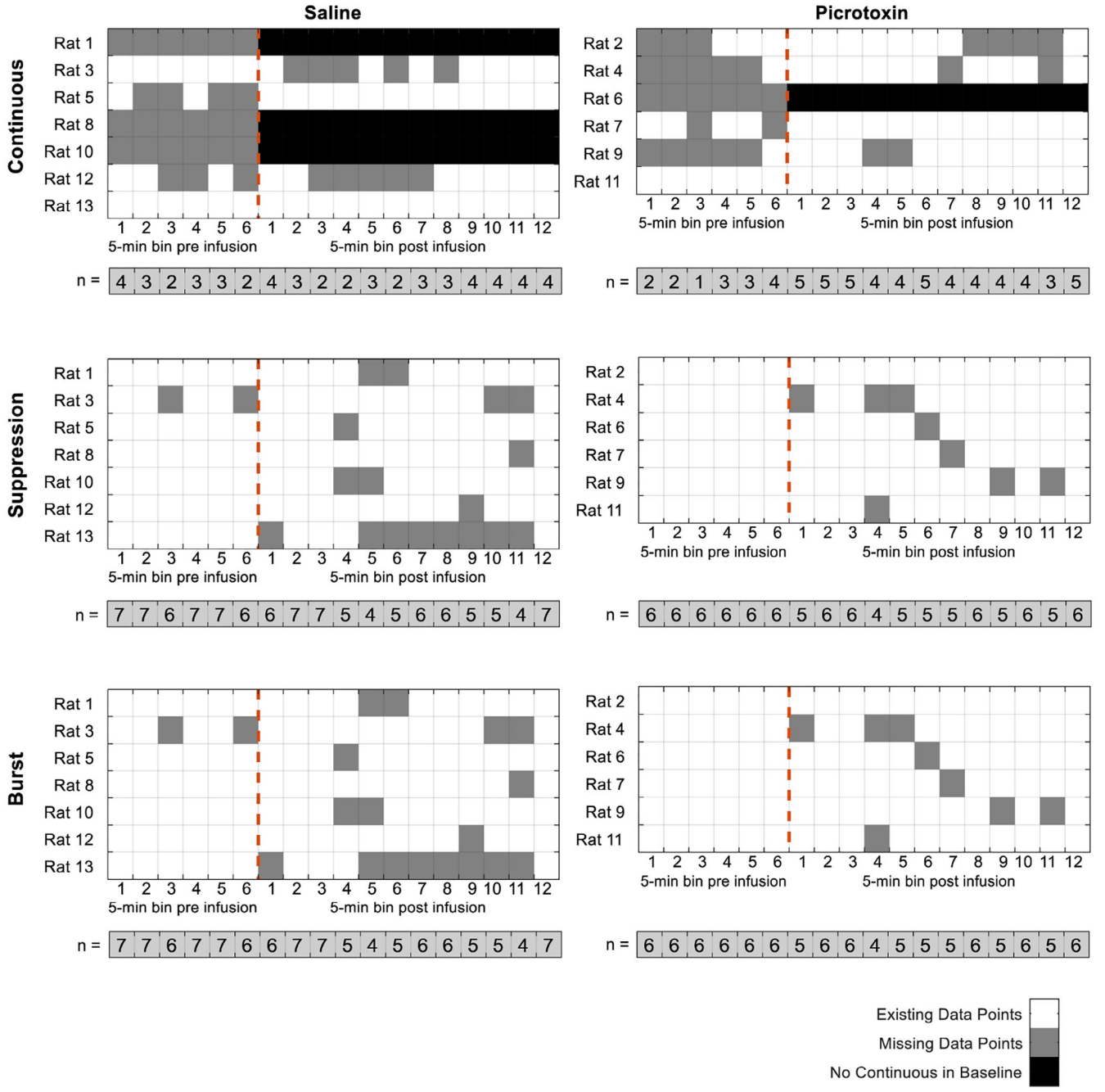

FIGURE 3 State-separated data available in saline and picrotoxin infusion groups for each of the six baseline and 12 post-infusion5-min bins. For each of the drug (saline or picrotoxin)-state combinations, a grid is shown to indicate missing data points, with the time bin on the *x*-axis and the rat ID on the *y*-axis. Underneath is the total number (*n*) of rats that contributed values for each 5-min bin in the different drug-state combination [Color figure can be viewed at wileyonlinelibrary.com]

In a final step, we further separated the burst-suppression state into the burst and suppression components, using a semiautomatic LFP-amplitude thresholding routine in Fieldtrip. To this end, a distribution of the absolute amplitude-values of the signal was formed. Samples that exceeded a fixed *z*-value of 5 and those falling within a symmetrical 0.25-s window around the threshold crossing were consecutively labeled as burst state. This thresholding was run on each individual channel to prevent summation of *z*-values, which could occur from synchrony across channels and convolute the routine. The output of this routine gave the boundaries between low amplitude activity, corresponding to the suppression state, and the burst state.

Not all rats were spending time in each of the LFP states for every 5-min bin of the recording period, and four rats were not spending any time in the continuous state during baseline (therefore not allowing baseline normalization of the post-infusion data). Therefore, the number of rats contributing to the different analyses of state-

separated data could differ from the overall number of rats from which recordings were made (Figure 3). The reduced sample size during the continuous state implies that the statistical power of any analysis in the continuous state is reduced compared to the analysis of the other two states.

2.3 | State-separated analyses of hippocampal LFP properties

2.3.1 | Power spectral density

Power at different frequencies was analyzed separately for the different LFP states in FieldTrip, using Fast Fourier Transform with a Hanning window from 0.5 to 40 Hz. These power spectra were subsequently averaged across channels and compared across the different states. Given the substantial raw-power differences between the different states (already separated in this analysis) and in order to investigate potential differences in relative spectral density, for each individual channel, we additionally normalized the spectra to the total area under the curve of the power spectrum before comparison across states.

2.3.2 | Connectivity

Phase-locking values (PLVs) were calculated to indicate the phase-coherence (a measure of neuronal synchronization that is independent of amplitude correlations) of two signals originating from a pair of electrodes (measuring local activity due to their bipolar montage; Aydore, Pantazis, & Leahy, 2013; Bastos & Schoffelen, 2015; Srinivasan, Winter, Ding, & Nunez, 2007). PLVs were calculated for every possible pair of hippocampal electrodes for every 0.5-Hz frequency bin. Because the individual electrodes between rats were not at consistent locations within the temporal to intermediate hippocampus, instead of averaging PLVs of electrode pairs across subjects (as is common in electroencephalography [EEG]/magnetoencephalography analysis where a standard mapping of electrodes does exist, for example, Oostenveld & Praamstra, 2001), we used a different method to extract the communality of connectivity between all electrode pairs and to then calculate a statistic of this across rats (Cohen, 2015). To this end, we used singular value decomposition (SVD) over the imaginary part of the PLV matrix of all states and times. We used the imaginary part of the complex PLV (complex cross-spectrum normalized on power in individual trials) as this is not corrupted by volume-conduction problems (Nolte et al., 2004). For each rat and frequency bin, we extracted the singular vectors U and V that satisfy the equation PLV = $U \times S \times V'$, with S being the matrix of singular values and PLV the matrix of imaginary PLVs. The individual imaginary PLV matrices for each state and time combination were then projected into this space using the respective singular vectors, and the first two "singular values" were extracted. These two values represent the connectivity strength within the two dominant "neural networks" of the rat in the area of the temporal to intermediate hippocampus sampled by the bipolar seven-electrode montage.

2.3.3 | Multi-unit activity

We compared the following key MUA parameters between LFP states: overall firing rate, bursts per minute, percentage of spikes in burst, and burst duration. The original MUA analysis in our previous study (McGarrity et al., 2017) had been completed using NeuroExplorer (version 4). However, in order to examine the state-dependency of MUA parameters (and, subsequently, also of the previously reported disinhibition-induced enhancement of MUA burst parameters, see below), we replicated the original analysis using MATLAB, where we could then separate the different snippets of MUA by their associated LFP state. The MUA data were separated according to the different LFP states based on their time stamps in a way that preserved the original MUA bursts, with each burst assigned to the state occupied longest during the burst duration.

2.3.4 | Statistical comparison of the three distinct hippocampal LFP states during baseline

To analyze the effect of the different states on the overall LFP and MUA, we compared the baseline data, removing the factor of drug. For the baseline frequency-specific effects (power spectra and PLV), we compared each state to both other states in a separate analyses, after running a moving average over the frequency values, with a kernel of 1.5 Hz sliding over 0.5 Hz. The statistical analysis of these effects was carried out using pairwise comparisons at each frequency bin. In order to address the multiple comparisons problem arising from the simultaneous analysis of 80 different frequency bins, we conducted a cluster permutation analysis (Hayasaka, Phan, Liberzon, Worsley, & Nichols, 2004; Maris & Oostenveld, 2007). This method runs a mass-univariate independent samples t-test for each frequency bin, for both real data pairs (of the conditions to be compared) and randomly assigned pairs (combining data of both conditions to obtain a reference distribution). Adjacent frequency bins that pass the univariate significance threshold form a cluster and a summary statistic of these clusters (e.g., summed t-value) is calculated for real data and reference distribution data. Only those clusters from the comparisons of the real data pairs which cutoff less than 5% of the maximum cluster statistic from the reference distribution (random pairs) were considered as statistically significantly different.

For the state-separated analysis of MUA, a problem of missing data points over time arose due to the limited time each rat spent in each state (see Figure 3 for the missing data in different 5-min bins). Therefore, it was not possible to conduct a repeated-measures analysis of variance (ANOVA) and so we used a pooling strategy. More specifically, we used the 5-min bins in the different states as the units of observation, such that data from all rats and time bins were pooled

according to state—after averaging across channels (for each rat). This was then subjected to a between-subjectsone-way ANOVA, with LFP state as the between-subjects factor; this reflects a fixed-effect analysis.

2.4 | Analyses of LFPstate-dependent drug infusion effects

2.4.1 | Power spectral density

For the comparison of frequency-specific effects of drug infusion, the difference between pre- and post-infusion power was expressed as log of the ratio between post-infusion (power spectra over 60 min) and pre-infusion (baseline; power spectra over 30 min) values for each channel. These difference values were then averaged per rat for statistical analysis, then for each drug group for plotting. The statistical analysis of the frequency-specific effects of picrotoxin compared to saline infusions on LFP power was carried out using cluster permutation where, separately for each LFP state, the log ratio of both drug groups was compared.

2.4.2 | Connectivity

The first two PLV "singular values" for each rat (see Section 2.3.2) were averaged to give a single measure of aggregate connectivity. To normalize post-infusion values to pre-infusion (baseline) values, the pre-infusion values were subtracted from the post-infusion values. As was done for the spectral power analysis, the cluster permutation statistic was used to compare the effects of picrotoxin vs. saline for each of the LFP states separately.

2.4.3 | Multi-unit activity

Our previous analysis, which did not separate MUA data according to LFP state, showed that hippocampal disinhibition by picrotoxin causes enhanced burst firing, as reflected by increased bursts per minute, percentage of spikes in burst, and burst duration (McGarrity et al., 2017). Therefore, our present analysis focused on these burst parameters.

To assess the effect of picrotoxin on the state-separated MUA analysis, we could not apply the mixed-model ANOVA of MUA parameters with drug as between-subjects and time (5-min bin) as repeated-measures factors, which we used in our original MUA data analysis (which did not separate data by LFP state; McGarrity et al., 2017). This is because of the many missing data points, following separation of data according to LFP state (see Figure 3). Therefore, we used the same pooled analysis as for the comparison of MUA parameters between LFP states during baseline, however, here with the additional factor of infusion group. Again, data were pooled over time and rats and separated according to LFP state and infusion group. Prior to pooling, data for each rat, in each state, were normalized by subtracting the average of the pre-infusion values for each channel from the individual post-infusion values for the corresponding channel; subsequent to this, an average was taken across the channels, for each rat and time point separately. The normalized and pooled MUA data were subsequently analyzed using a two-way ANOVA, with LFP state and infusion condition as between-subjects factors (and time bins and rats as units of observation). A significant infusion condition × state interaction would statistically support state-dependent drug effects.

3 | RESULTS

3.1 | Three distinct hippocampal LFP states under isoflurane

3.1.1 | Differences in frequency-dependent power and functional connectivity

To compare quantitatively the three distinct hippocampal LFP states (Figure 1a), we combined the baseline data (i.e., data recorded before any drug infusion) from all infusion groups. During the baseline period, all rats showed the burst and suppression states, but not all rats showed a continuous state, resulting in a sample size of $n = 13$ rats for the burst and suppression state and of $n = 9$ rats for the continuous state (Figure 3).

The three LFP states substantially differed with respect to overall raw power and with respect to relative power at different frequencies (Figure 4). The overall raw power in the burst state was significantly and substantially higher than in the suppression (cluster level $p = .000999$, corrected for multiple comparisons; cluster spanning across all frequencies, that is, 1–39 Hz) and continuous states ($p = .005$, cluster including 1–22.5 Hz). Suppression and continuous states did not differ significantly ($p > .05$) indicating similar overall power, although at lower frequencies power tended to be somewhat higher in the continuous compared to the suppression state (Figure 4a). With respect to relative power at different frequencies, the burst state showed a higher proportion of power within delta/low theta than the other two states and tended to show a lower proportion of power in high frequencies from about 20 to 40 Hz than both the suppression and continuous states, which were both characterized by conspicuous gamma "bumps" in the normalized power spectra in this frequency range (Figure 4b). For the comparison between burst and continuous states, a significant cluster was found at 3.5–10 Hz ($p = .024$), and between burst and suppression states a significant cluster was found at 4–14 Hz ($p = .009$). The numerical differences at higher frequencies did not reach statistical significance: neither for the comparisons of continuous and burst states ($p = .16$) nor suppression and burst states ($p = .10$).

Regarding connectivity, we computed an aggregate measure of phase-locking between all electrode pairs spread across the temporal to intermediate hippocampus (see Section 2). To exclude any

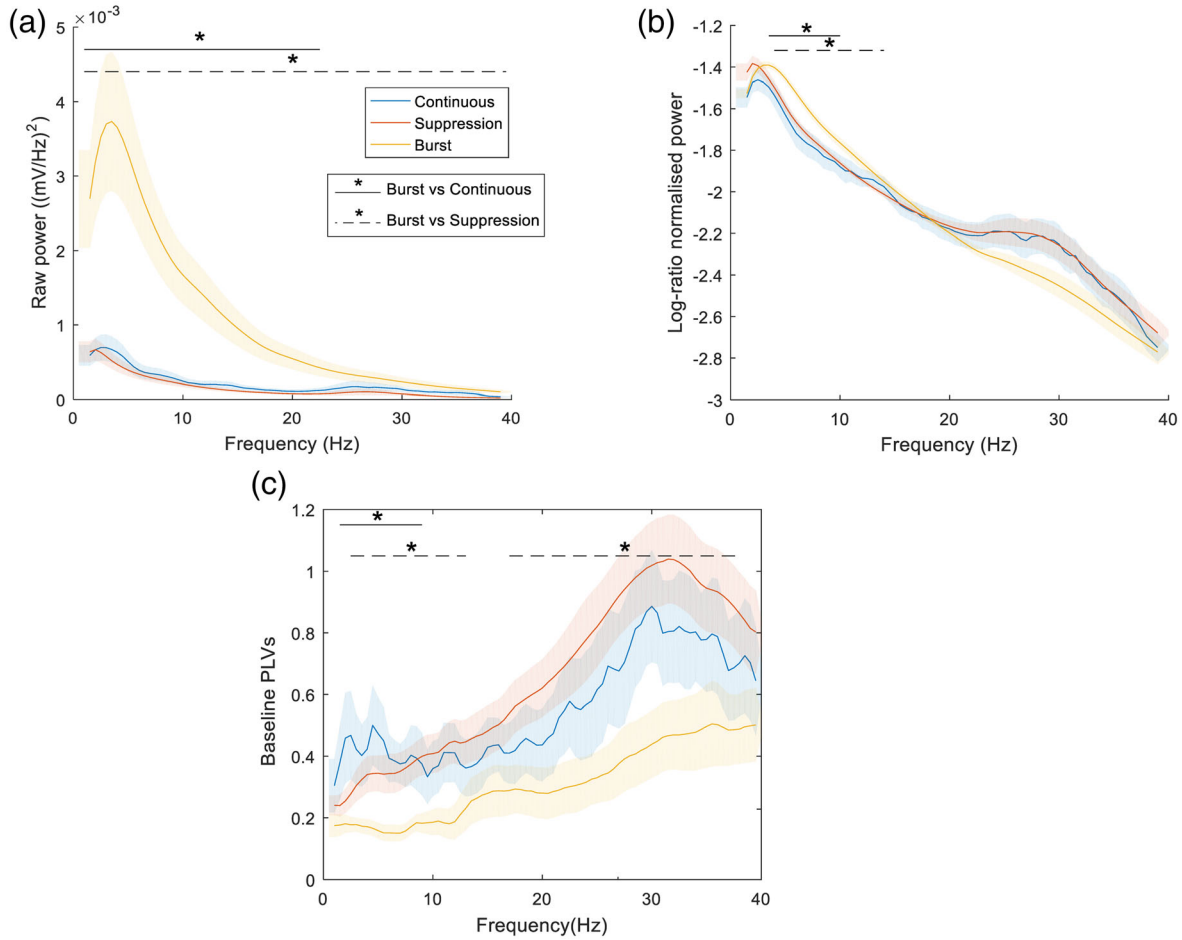

FIGURE 4 The three hippocampal local field potential (LFP) states—differences in frequency-dependent power and connectivity. (a) Raw power spectral density, (b) log-ratio of power divided by the total area under the curve (representing relative power at different frequencies), and (c) phase-locking values (PLVs) are shown across frequencies for each of the three LFP states. All values are shown as mean ± SEM. The frequency ranges showing significant ($p < .05$) differences based on cluster permutation statistics are indicated by an asterisk (*) and a solid line for comparisons between burst and continuous, and a dashed line for comparisons between burst and suppression states. Number of rats contributing data to the different states: burst, $n = 13$; suppression, $n = 13$; continuous, $n = 9$ [Color figure can be viewed at wileyonlinelibrary.com]

contamination by volume conduction, only the imaginary part of the PLVs was used and submitted to an SVD, of which we report the first two diagonal (Eigen-)values. Across the frequency range examined (0.7 to 40 Hz), the burst state showed generally lower connectivity than both suppression and continuous states, which showed very similar connectivity (Figure 4c). One significant cluster was found for the comparison between burst and continuous states at 1.5–9 Hz ($p = .018$), and two significant clusters for the comparison between burst and suppression states: one cluster at 2.5–13 Hz ($p = .019$) and another cluster at 17–38 Hz ($p = .005$). In all these clusters, connectivity was reduced in the burst state, in comparison to both the continuous and the suppression state.

Overall, in terms of total power, relative power at different frequencies and functional connectivity, the burst state of the hippocampal LFP markedly differs from the suppression and continuous states, whereas the latter two states show similar characteristics in these parameters.

3.1.2 | Differences in associated MUA

At baseline, some of the MUA parameters differed between states (Table 1), consistent with the impression based on visual inspection of hippocampal recordings (Figure 1a). The pooled analysis explained in the methods revealed that states significantly differed with respect to overall firing rate (spikes per second) ($F[2,180] = 3.37$, $p = .037$), with the firing rate in the burst state being higher or tending to be higher, respectively, than in the suppression state ($p = .02$) and continuous state ($p = .058$), which did not differ ($p = .904$). States also differed significantly with respect to percentage spikes in burst ($F[2,177] = 9.44$, $p < .0001$), with both burst and continuous states, which did not differ significantly ($p = .108$), showing a higher percentage of spikes in bursts than the suppression state ($p = .002$ and $p < .0001$, respectively). States did not differ significantly with respect to bursts per minute ($F[2,177] = 0.95$, $p = .383$) or burst duration ($F[2,172] = 1.19$, $p = .307$). Overall, this quantitative comparison of MUA parameters is consistent

with the impression based on visual inspection of the MUA data in the three states (Figure 1a) that MUA activity is "suppressed" in the suppression state compared to the burst and continuous state. It should be noted that, although these differences were suggested by visual inspection of most recordings, they were not always apparent even in recordings from different electrodes in the same rat. For example, in Figure 1a burst and suppression states clearly show higher MUA on Channel 1 whereas on Channel 2, which shows a higher overall firing rate, the states display similar MUA, possibly reflecting a ceiling effect.

3.2 | Hippocampal neural disinhibition did not affect the expression of the three hippocampal LFP states

During the post-infusion period, the cumulative time spent in the different LFP states was similar in rats infused with picrotoxin and saline (Figure 5). Independent sample *t*-tests revealed that there was no significant difference between the picrotoxin and saline groups in the total time spent in any of the three LFP states (continuous state, $t(7) < 1$; suppression and burst state: $t(11) < 1$).

3.3 | Hippocampal neural disinhibition caused state- and frequency-dependent effects on hippocampal LFP power and functional connectivity

Hippocampal picrotoxin infusions, compared to saline, tended to increase power in the lower frequencies (<20 Hz) and to decrease power in the higher frequencies (>20 Hz), in both burst and suppression states, while having minimal effect in the continuous state (Figure 6a, c, e). However, only the picrotoxin-induced increase in power at 6–18 Hz in the burst state attained statistical significance ($p = .017$). In the continuous state, power was numerically higher during the post-infusion period, as compared to the pre-infusion baseline; this was regardless of infusion, as indicated by a positive difference in log ratio power, especially at lower frequencies, which indicates "baseline drift." There was no difference between the drug groups in this state (no clusters; Figure 6a).

Hippocampal picrotoxin tended to decrease functional connectivity (as reflected by PLVs) at higher frequencies in the burst and suppression states and at lower frequencies in the continuous state (Figure 6b, d, f). However, the picrotoxin-induced decreases in connectivity reached statistical significance only in the burst state, in a high-frequency cluster ranging from 29.5 to 33 Hz ($p = .049$), but there was no significant picrotoxin-induced decrease in connectivity during the suppression state (no clusters). The visually apparent decrease in the continuous state (at lower frequencies) also failed to reach statistical significance, although there was a trend in a cluster from 6 to 7 Hz ($p = .065$).

3.4 | State-dependence of enhanced multi-unit burst firing caused by hippocampal neural disinhibition

We first replicated the picrotoxin-induced increases in burst parameters, including bursts per minute, percentage of spikes in bursts and burst duration, as calculated by the Neuroexplorer software and originally reported by McGarrity et al. (2017), using a MATLAB code that could be run with the segmented LFP state-separated data (Figure 7a–c); the original Neuroexplorer data for rats that were excluded from the LFP analysis (see Section 2.1) was inputted directly into MATLAB to complete the data set for comparison of analyses (i.e., $n = 8$ rats in the picrotoxin group and $n = 7$ rats in the saline group). Next we plotted the time course of the multi-unit burst parameters following picrotoxin and saline infusions separately for the three different LFP states, using the state-separatedmulti-unit data

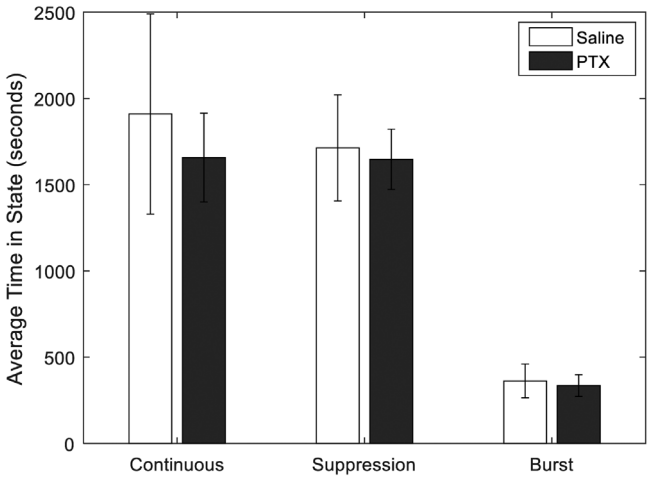

FIGURE 5 Hippocampal neural disinhibition does not affect the expression of the three hippocampal local field potential (LFP) states. Cumulative time (mean ± SEM) spent in each LFP state by the two drug groups during the post-infusion period

TABLE 1 Baseline values for different multi-unit activity bursting parameters in the three local field potential states

	Bursts per minute	% spikes in burst	Mean burst duration (s)	Spikes per second
Continuous	441.50 ± 65.95	35.10 ± 2.22*2	0.0094 ± 0.00025	21.29 ± 5.12
Suppression	325.85 ± 47.75	20.26 ± 1.96 *1,*2	0.0088 ± 0.00039	24.06 ± 3.16*1
Burst	380.32 ± 44.03	29.26 ± 2.14*1	0.0093 ± 0.00041	65.33 ± 18.86*1

Note: Mean ± SEM. * indicates significant difference between states ($p < .05$), with the number indicating the pair of states that differ.

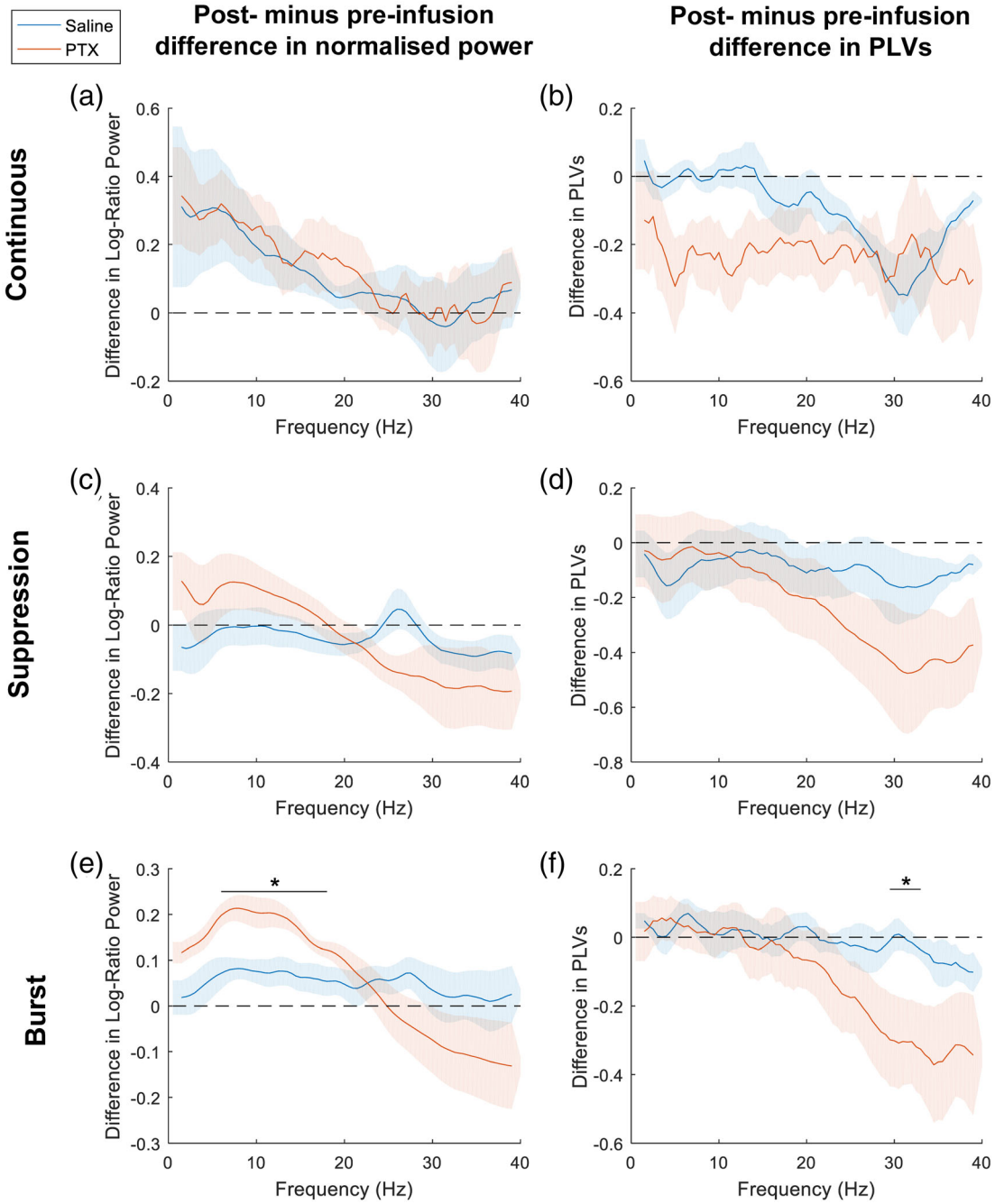

FIGURE 6 Hippocampal neural disinhibition causes state- and frequency-dependent effects on hippocampal local field potential power and functional connectivity. Frequency-dependent impact of hippocampal picrotoxin or saline infusion on power (left) and on functional connectivity (right) in the continuous (top panel), suppression (middle panel), and burst (bottom) states. The logarithm of the ratio between post-infusion (saline or picrotoxin) and pre-infusion (baseline) power is shown as a measure of their respective "difference" for both infusion groups across frequencies and separately for each state (a, c, e). The difference between post-infusion (saline or picrotoxin) and pre-infusion (baseline) phase-locking values (PLVs) as a measure of aggregate functional connectivity is shown for both infusion groups across frequencies and separately for each state (b, d, f). All values are shown as mean ± SEM. The dotted line (value of 0) represents no change from the pre- to the post-infusion period, while positive numbers indicate an increase from baseline and negative numbers a decrease from baseline in the post-infusion period. The frequency ranges showing significant ($p < .05$) differences between the picrotoxin and saline infusion groups based on cluster permutation statistics are indicated by an asterisk (*) and a solid line [Color figure can be viewed at wileyonlinelibrary.com]

(Figure 7d–l) (with sample sizes for the different 5-min bins indicated in Figure 3). Visual inspection of these plots indicates that, numerically, the picrotoxin-induced increase of bursts per minute appears to be weaker during the continuous LFP state (Figure 7d-f) compared to the burst state (Figure 7g–i) and suppression state (Figure 7j–l). In order to examine directly the LFP state-dependence of the picrotoxin

effects, we pooled the time-deconstructedpost-infusion values of the three multi-unit burst parameters, subtraction-normalized to baseline, and separated them by infusion group and LFP state (Figure 7m–o). ANOVA of these values, using LFP state and drug infusion as independent variable (see Section 2.4.3), revealed a significant main effect of drug infusion for all three burst parameters (outcomes of statistical analysis not shown), reflecting that, overall, picrotoxin infusion increased these values as compared to saline infusion. Importantly,

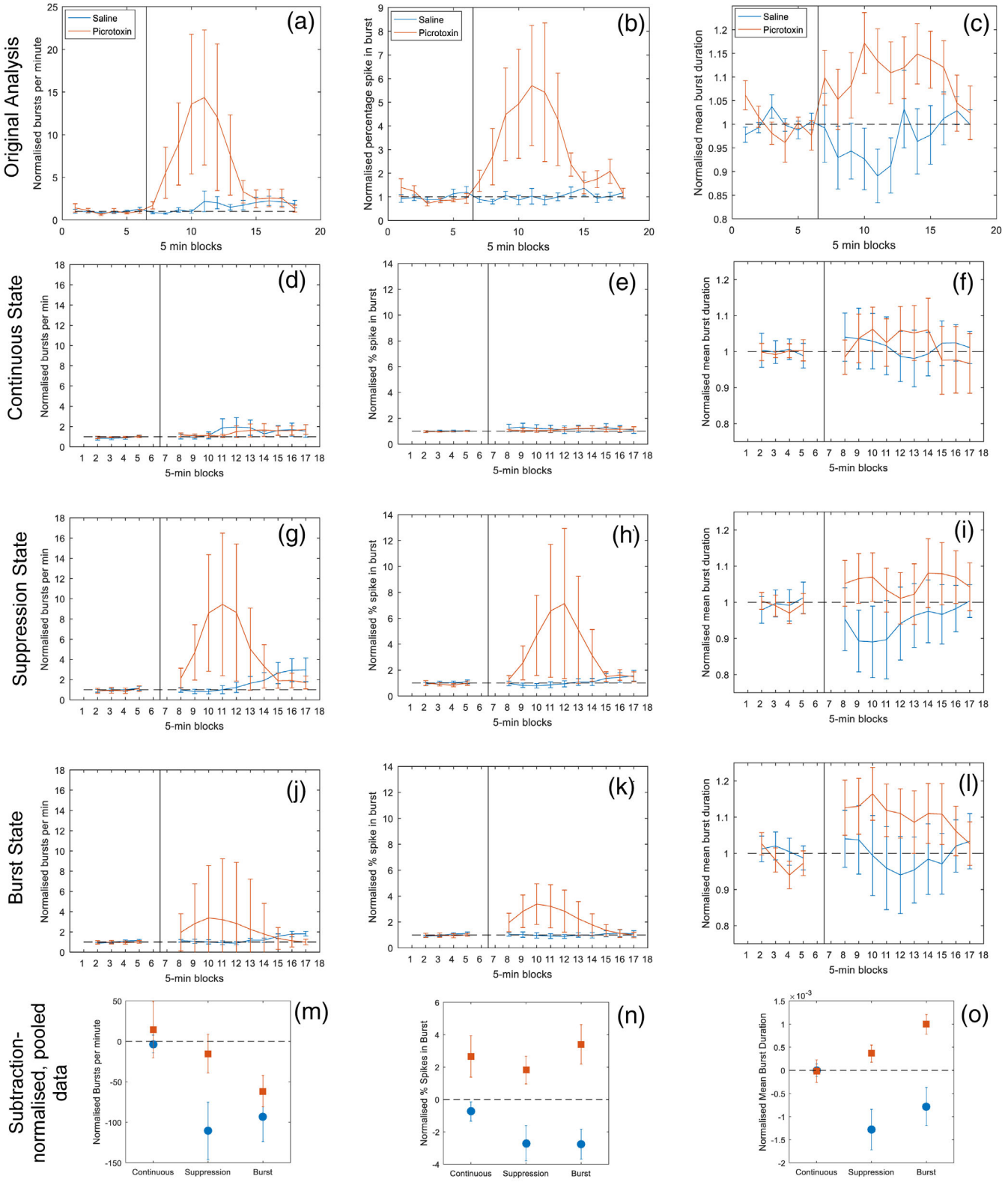

FIGURE 7 Legend on next page.

the ANOVA of burst duration (Figure 7o) revealed a significant interaction of drug infusion x LFP state (F[2,316] = 3.86, p = .022), reflecting that picrotoxin increased burst duration in the burst and suppression states, but not the continuous state. Although, numerically, the picrotoxin-induced increases in bursts per minute and percentage of spikes in bursts also tended to be somewhat weaker in the continuous, compared to the other two states (Figure 7m,n), ANOVA did not support significant interactions of drug infusion×LFP state for these two parameters (burst per min: F(2,343) = 1.118, p = 0.328; percentage spikes in bursts: F(2,343) <1). Overall, the increased multi-unit burst duration following hippocampal neural disinhibition was markedly less pronounced in the continuous state of the hippocampal LFP, as compared to the other two states. The other two burst parameters showed numerical tendencies in the same direction, but these were not statistically significant.

4 | DISCUSSION

We, first, developed a semi-automated method based on the kurtosis of the LFP peak-amplitude distribution and amplitude envelope thresholding to separate three distinct hippocampal LFP states in the isoflurane anesthetized rat: burst, suppression, and continuous states (Figure 1), and we described some of the properties of these three LFP states. The burst state shows substantially larger overall raw power across the frequency range examined compared to the suppression and continuous states (Figure 4a), as well as higher relative power in the delta/theta range (<15 Hz), but lower relative power in the high beta/low gamma range (>20 Hz) (Figure 4b). Moreover, compared to suppression and continuous states, the burst state showed lower frequency-specific "functional connectivity" across the recording area in the temporal to intermediate hippocampus, as reflected by reduced phase-locking values of the LFP signals recorded from the different electrodes (Figure 4c). In terms of MUA, overall neuronal firing was higher in the burst state than in the two other states, whereas the percentage of spikes fired in bursts was higher in both the burst and continuous states as compared to the suppression state (Table 1). Finally, the expression of the hippocampal LFP states, as reflected by the cumulative duration of these states across the recording period, was not affected by hippocampal neural disinhibition (Figure 5).

Second, and importantly, we then showed that hippocampal neural disinhibition by picrotoxin changed the hippocampal LFP in a state- and frequency-dependent way (Figure 6). In both burst and suppression states, but not the continuous state, hippocampal neural disinhibition tended to increase LFP power at lower frequencies (<20 Hz) and to decrease power and functional connectivity at higher frequencies (>20 or >15 Hz, respectively). There was also a trend toward picrotoxin decreasing functional connectivity in the theta range (6–7 Hz) during the continuous state.

Third, we also found that the increase in multi-unit burst parameters by hippocampal neural disinhibition, which we reported in a previous study (McGarrity et al., 2017), was partially dependent on the hippocampal LFP state: disinhibition-induced increases in burst duration were limited to the burst and suppression state and not apparent in the continuous state (Figure 7).

4.1 | Three distinct hippocampal LFP states under isoflurane anesthesia

Visual inspection of the LFP recorded from the temporal to intermediate hippocampus in isoflurane-anesthetized rats indicates three distinct LFP states, including burst, suppression, and continuous states (Figure 1a). We found that the kurtosis of the LFP peak and trough amplitude distribution was the best metric to separate the periods including burst and suppression states from the continuous state. Using this kurtosis measure, we thus separated the continuous state from the combined burst and suppression states, which could then be separated by amplitude envelope thresholding. Power analysis corroborated the impression based on visual inspection of the LFP traces that raw power during the burst state is substantially higher than in the other two states, owing to large amplitude LFP bursts, and that the continuous state tends to show higher power than the suppression state (although the latter difference failed to reach statistical significance). Interestingly, analysis of relative power revealed a marked beta/gamma shoulder (24–34 Hz) in the power spectra of continuous and suppression states which was absent in the burst state. Others

FIGURE 7 State-dependence of enhanced multi-unit burst firing caused by hippocampal neural disinhibition. The top row displays a replication of the time course of multi-unit burst parameters during baseline and following infusion of picrotoxin and saline, across all local field potential (LFP) states, that is, without state separation, as originally reported by McGarrity et al. (2017), but carried out in MATLAB rather than Neuroexplorer v4. Hippocampal neural disinhibition by picrotoxin markedly enhanced hippocampal multi-unit burst firing as compared to saline infusions, as reflected by increases in (a) bursts per minute, (b) percentage spikes in burst, and (c) burst duration (and statistically supported by a significant infusion × time interaction, McGarrity et al., 2017). All values are division-normalized to the baseline value and mean ± SEM. The three rows underneath display the same time course analysis, but separated by LFP state, using the MATLAB scripts developed in the present study: (d–f) continuous state; (g–i) suppression state; and (j–l) burst state. Visual inspection indicates that the picrotoxin-induced enhancement of burst parameters is less pronounced in the continuous, compared to the other two states. To visualize the potential interaction of hippocampal infusion and LFP state, the bottom row displays the time-deconstructed and pooled post-infusion values (subtraction-normalized to baseline, mean ± SEM) of (m) burst per min, (n) percentage spikes in bursts, and (o) burst duration (seconds), for the picrotoxin and saline infusion groups and separated by LFP state; these plots also indicate that the picrotoxin-induced increase in burst parameters is, at least numerically, less pronounced in the continuous than in the other two states [Color figure can be viewed at wileyonlinelibrary.com]

TABLE 2 The continuous and the burst and suppression states of the hippocampal local field potential (LFP) in isoflurane-anesthetized rats in comparison to previously described hippocampal and cortical LFP states under anesthesia

Source	"Continuous" state	"Burst" and "suppression" states	Additional comments
Clement et al., 2008	**State referred to as**: Activated State **LFP pattern**: "Activated EEG patterns consisted of low amplitude fast activity at neocortical sites concomitant with theta (rhythmic 3–5 Hz) activity at hippocampal sites" **Unit activity**: Not reported	No equivalent state reported	**Species**: Rats **Anesthesia**: Urethane **Recording area**: Hippocampus A hippocampal slow oscillation state (see Wolansky et al., 2006, from the same research group) is mentioned
Ferron, Kroeger, Chever, & Amzica, 2009	**State referred to as**: Low-Isoflurane **LFP pattern**: [EEG] "All recording sessions started under 1.5% isoflurane anesthesia, which produced activity patterns comparable to those recorded during slow-wave sleep (SWS) and under ketamine-xylazine anesthesia (figure 1A) … Briefly, these patterns consist of a quasi regular slow oscillation with a frequency range just below 1 Hz." **Unit activity**: Not reported	**State referred to as**: Burst-Suppression **LFP pattern**: [EEG] "[A] deep level of anesthesia, producing burst suppression (BS), generates a state of unstable cortical hyperexcitability… BS is an electroencephalographic (EEG) pattern consisting of an alternating pattern of (1) epochs with silenced cortical activity and associated EEG isoelectric line, and (2) periods displaying high-amplitude slow and sharp waves" **MUA**: [Intracellular Recordings] "The EEG patterns during BS consisted of periods of bursting and isoelectric lines. During the latter, all recorded cortical neurons displayed a hyperpolarized membrane potential devoid of any synaptic activity, whereas bursts consisted of depolarizing triangular-shaped potentials, synchronous with corresponding field and EEG waves"	**Species**: Cats **Anesthesia**: Isoflurane **Recording area**: Neocortex It is unclear how this SWS mentioned here relates to our activated state, as the isoflurane level (1.5%) is higher than we, and others, report for similar states. It may be a state which is part of the transition from our activated to deactivated state
Kroeger & Amzica, 2007	**State referred to as:**Low-Isoflurane/SWS **LFP pattern:** [EEG] "Lower doses (1–2% isoflurane), sufficient for painless surgical procedures, produced a pattern of continuous Sleep-like slow waves" **Unit activity:** Not reported (in the absence of stimulation)	**State referred to as:**Burst-suppression **LFP pattern:** [EEG] "[A] state of deep anesthesia induced by various anesthetics (isoflurane, barbiturates, and propofol) associated with an electroencephalographic pattern of BS… BS was obtained with higher doses of anesthetic (in the case of isoflurane, 2%), and its patterns, in accordance with previous descriptions, were characterized at the EEG level by alternating periods of (1) bursts of high-amplitude and low-frequency (15 Hz) waves, and (2) isoelectric EEG." **MUA:** [Intracellcular Recordings] "This further supports the claim that the state of BS is a state of hyperexcitability. The onset of this state window is prefigured by a progressive increase in the extracellular Ca2+ concentrations that may, on the one hand, transiently enhance cortical synaptic processes, and, on the other hand, reduce spontaneous firing of neurons through enhanced	**Species:** Cats **Anesthesia:** Isoflurane **Recording area:** Neocortex See comments above for Ferron et al., 2009 relating to the low-isoflurane state

(Continues)

TABLE 2 (Continued)

Source	"Continuous" state	"Burst" and "suppression" states	Additional comments
		screening of Na + channels … thus contributing to the gradual onset of suppression episodes"	
Land et al., 2012	**State referred to as:** Light anesthesia/low suppression **LFP pattern:** "After the decrease of isoflurane concentration to 0.7 vol … activity to finally return into the initial state of small amplitude LFP activity." "The light anesthesia state was characterized by theta oscillations in the subiculum with a mean peak frequency of 4.8 Hz (SD 0.3 Hz)" **MUA:** "After the decrease of isoflurane concentration to 0.7 vol %, this sequence of events appeared in reversed order: suppression was followed by burst-suppression, then slow rhythmic activity to finally return into the initial state of small amplitude LFP activity … Multiunit activity in V1 and the subiculum followed these changes in LFP activity [in this order or in reverse] with analogous changes in spiking patterns"	**State referred to as:** Deep anesthesia/high suppression/burst-suppression **LFP pattern:** "Increasing levels of anesthesia eventually produce burst suppression of cortical activity, a pattern of alternating high amplitude bursts and periods of suppressed activity (silent periods) signifying deep anesthesia" "In anesthesia-inducedburst-suppression, the duration of silent periods between bursts is dose-dependent" "The deep anesthesia state was characterized by regular slow rhythmic burst-suppression in the subiculum, with a mean peak frequency of 0.17 Hz (SD 0.05 Hz)" **MUA:** "LFP bursts in V1 or the subiculum were always accompanied with bursts of strong multiunit activity at the respective electrode sites"	**Species:** Mice **Anesthesia:** Isoflurane **Recording area:** Hippocampus
Lustig et al., 2016	**State referred to as:** Light isoflurane state **LFP pattern:** "Recordings during the lighter level of isoflurane anesthesia (~1%) consistently displayed a slow oscillation with a peak frequency of 3.4 Hz ± 0.57 Hz" "The depth profile of the running associated theta oscillations was strikingly similar to the slow oscillation during the light isoflurane state (3.5 Hz)." "[D]uring the light isoflurane state, we observed a slow, theta-like oscillation in CA1 and a faster, gamma-like oscillation around DG." **Single unit activity:** "[A]ctivity of neurons recorded in the CA1 and DG layers was modulated by theta-like and gamma-like oscillations, respectively"	**State referred to as:** Deep isoflurane state **LFP pattern:** "Under a deeper level of isoflurane anesthesia (2%), hippocampal activity was dominated by an oscillation with a peak frequency of 11.18 Hz ± 0.1 Hz" "[T]he depth profile of SPWs [sharp wave ripples] during water reward and quiet … was strikingly similar to the individual cycles of the 11 Hz oscillation during the deep isoflurane state" "In addition to these fast oscillatory events, we frequently observed randomly interspersed sharp LFP spikes in the D3 region" **Single unit activity:** "Firing in both CA1 and CA3 neurons was strongly phase locked to the individual cycles (figure 4C, top). CA1 neurons tended to fire a burst of action potentials around the trough of each cycle"	**Species:** Rats **Anesthesia:** Isoflurane **Recording area:** Hippocampus "We found that under different levels of isoflurane anesthesia activity in the hippocampus of rats displays two distinct states, which have several qualities that mirror the theta and LIA states"
Pagliardini, Gosgnach, & Dickson, 2013	**State referred to as:** Activated or REM-like **LFP pattern:** "The REM-like state was characterized by high power in the theta frequency bandwidth (range: 3.5–4.5 Hz) with a corresponding increase in power through the	No equivalent state reported	**Species:** Mice **Anesthesia:** Urethane **Recording area:** Hippocampus A hippocampal slow oscillation state (see Wolansky et al., 2006,

TABLE 2 (Continued)

Source	"Continuous" state	"Burst" and "suppression" states	Additional comments
	gamma band (25–40 Hz), consistent with the expression of gamma activity during both natural sleep and during anesthesia in previous studies" **Unit activity:** Not reported		from the same research group) is mentioned
Steriade, Amzica, & Contreras, 1994	No equivalent state reported	**State referred to as:** Burst-suppression **LFP pattern:** "The EEG pattern of burst-suppression that followed administration of various anesthetics generally consisted of sharp waves with high amplitudes, at frequencies usually ranging between 2 and 7 Hz, separated by progressively longer periods of complete flatness. The electrical silence lasted for 1–2 sec during the initial stage of this pattern (fig. 1A3), but reached 5–15 sec in later stages (figures 1A, 4, and 2C) and even 30 sec or more in some instances (see below, figures 7 and 9A)" **Unit activity:** [Extra- and Intra-cellular recordings] "'Only 60-70% of them (11 RE thalamic and 20 thalamocortical cells) ceased firing before the occurrence of burst-suppression; thereafter, those cells discharged during EEG wave bursts and were completely silent during flat periods of the EEG"	**Species:** Cats **Anesthesia:** Mixture of various anesthetics, including urethane (background anesthesia), ketamine, or xylazine and ketamine, nitrous oxide (N20), and sodium pentobarbital **Recording area:** Neocortex and thalamus
Wolansky et al., 2006	**State referred to as:** Activated state or theta state **LFP pattern:** "The activated state [during sleep] consists of prominent 3–12 Hz rhythmical activity known as theta or rhythmic slow activity." "[T]he same electrographic could be observed during spontaneous state changes under urethane anesthesia" "Under urethane, [Slow Oscillation state, see Additional comments] … appeared to be dependent on the level of anesthesia; increasing anesthetic dosage moderately increased the proportion of time spontaneously spent in the slow oscillatory state (correspondingly decreasing the amount of time spontaneously spent in theta)" **Single unit activity:** "Most of the neurons that generated rhythmic action potentials during the SO also did so during theta"	No equivalent state reported	**Species:** Rats **Anesthesia:** Urethane **Recording area:** Hippocampus Wolansky et al. reported a Hippocampal Slow Oscillation state at 1 Hz with a strong gamma power. It is unclear how this relates to our states, but it is not directly comparable to our burst-suppression state

Note: The direct quotations highlight state properties corresponding to the "continuous" and the "burst" and "suppression" states shown in the present study. Additional comments regarding the authors' interpretation of these states, and any comments on the relation to the states described in the present study, are shown in the "Additional Comments" column.
Abbreviation: MUA, multi-unit activity.

have previously reported similar beta/gamma shoulders in the hippocampal LFP during continuous-like LFP states under anesthesia (Land et al., 2012, *isoflurane*; Pagliardini, Gosgnach, & Dickson, 2013, *urethane*). However, if the burst state is not separated from the other LFP states, hippocampal LFP power spectra recorded under anesthesia do typically not show a beta/gamma shoulder (Lustig et al., 2016, and our unpublished observations, *both isoflurane*). This likely reflects that the power spectra are dominated by the large-amplitude burst state (which lacks a beta/gamma shoulder). Overall, in the frequency range examined, continuous and suppression states tended to show higher connectivity, as indicated by PLVs, than the burst state across the recording area in the temporal to intermediate hippocampus. In the continuous state, a peak in connectivity was apparent at lower frequencies (<10 Hz, Figure 4c), which included the theta range, although statistically connectivity in this range did not significantly differ between continuous and suppression states. The numerically increased theta-range connectivity may correspond to findings of characteristic activity in the theta range in related hippocampal LFP states identified by others (Table 2). More specifically, several studies have described hippocampal LFP states under anesthesia, distinct from periods characterized by burst-suppression patterns and referred to as "light anesthesia" states (Land et al., 2012; Lustig et al., 2016, *both isoflurane)* or "continuous"/ "activated" states (Clement et al., 2008; Wolansky et al., 2006, *both urethane*), with distinct activity in the theta range (3–12 Hz), although these studies did not examine connectivity within the hippocampal recording area at the frequencies we investigated. These previous studies, which all recorded from the septal (also known as dorsal) hippocampus, showed a more distinct theta peak compared to our recordings, which were from the temporal to intermediate hippocampus. This is consistent with the septo-temporal reduction in theta power that has been reported by studies in freely moving and sleeping rats (Patel, Fujisawa, Berenyi, Royer, & Buzsaki, 2012; Royer, Sirota, Patel, & Buzsaki, 2010).

The three hippocampal LFP states differ with respect to the associated MUA. The burst state showed higher overall neuronal firing, as indicated by increased overall firing rate, than the suppression and continuous states. In addition, both burst and continuous state showed stronger burst firing than the suppression state, as reflected by a higher percentage of spikes in burst. Increased neuronal firing in the burst compared to the suppression state under isoflurane anesthesia has been reported previously in neocortical regions (Ferron et al., 2009; Kroeger & Amzica, 2007; Steriade et al., 1994) and in the subiculum (Land et al., 2012). To explain this difference, it was proposed that anesthesia induces a hyperexcitable state with an increased extracellular Ca2+ concentration. During the burst state, the high Ca2+ would facilitate synaptic transmission causing the Ca2+ to move into the neuron, which would then lead to the suppression state, a refractory period during which Ca2+ concentration is relatively high within (and relatively low outside) of the neurons, therefore decreasing the likelihood of neuronal activity until the Ca2+ is transported back into the extracellular space (Ferron et al., 2009; Kroeger & Amzica, 2007). In contrast, urethane anesthesia does not cause such a hyperexcitable state but instead reduces overall neural excitability by causing neural hyperpolarization (Ferron et al., 2009; Hara & Harris, 2002; Pagliardini, Funk, & Dickson, 2013). This may explain why under urethane anesthesia the hippocampal LFP does not show a burst-suppression pattern but is instead characterized by a slow oscillation of about 1 Hz (Clement et al., 2008; Land et al., 2012; Pagliardini, Funk, et al., 2013, Pagliardini, Gosgnach, et al., 2013; Wolansky et al., 2006).

Taken together, our semi-automated separation method based on the kurtosis of the LFP amplitude distribution revealed three distinct hippocampal LFP states under isoflurane anesthesia—burst, suppression, and continuous state—whose properties correspond to those of similar hippocampal LFP states under anesthesia that had been identified previously based on visual inspection or other methods (Table 2). In unanesthetized animals, that is, awake or sleeping, the hippocampus (and other brain areas) also show distinct LFP states that are characterized by the relative dominance of activity in different frequency bands and are associated with different neural firing patterns (Kay & Frank, 2019). Distinct unanesthetized LFP states resemble distinct anesthetized LFP states in terms of relative dominance of specific frequency bands and other properties (e.g., Lustig et al., 2016), although correspondence between specific anesthetized and unanesthetized LFP states is limited, not least because a defining feature of unanesthetized LFP states is their close association with specific behavioral states (Kay & Frank, 2019). Our study of picrotoxin-induced changes in the hippocampal LFP under isoflurane allowed us to examine these changes separately from behavioral effects of hippocampal disinhibition, including locomotor changes (McGarrity et al., 2017) which are known to affect the hippocampal LFP (Kay & Frank, 2019). On the other hand, isoflurane may interact with picrotoxin, limiting the generalizability of our findings to unanesthetized animals; at an anesthetic doses, isoflurane primarily acts as a positive allosteric modulator of GABA-A receptors, enhancing the amplitude and duration of GABA's effects at this receptor (Garcia, Kolesky, & Jenkins, 2010). Isoflurane, thereby, may counteract some of the effects of disinhibition by picrotoxin, a noncompetitive GABA-A receptor antagonist blocking the receptor's chloride channel (Olsen, 2006). In hippocampal neurons, picrotoxin has been shown to reduce both phasic and tonic GABA-A receptor currents (Bai et al., 2001), whereas isoflurane specifically enhances phasic GABA-A currents (Bieda, Su, & MacIver, 2009). Nevertheless, we have shown previously that hippocampal picrotoxin disinhibition enhanced hippocampal multi-unit bursting under isoflurane anesthesia, consistent with similar effects of hippocampal disinhibition in vitro and in unanesthetized rodents (see discussion in McGarrity et al., 2017) and, as discussed below, LFP changes observed in the present study were consistent with previous in vitro findings. This supports that electrophysiological studies under isoflurane anesthesia can reveal key neural effects of picrotoxin disinhibition in the hippocampus that are relevant to unanesthetized animals. In the present study, the cumulative duration of each of the three hippocampal LFP states under isoflurane was not affected by local infusion of the GABA-A receptor antagonist picrotoxin, indicating that the expression of the states does not

depend on GABA-Areceptor-mediated inhibition in the hippocampus. However, as discussed in the next two sections, hippocampal neural disinhibition by picrotoxin changed the LFP properties within the three hippocampal LFP states.

4.2 | State- and frequency-dependent changes in the hippocampal LFP power by local picrotoxin disinhibition

In both burst and suppression states, picrotoxin, as compared to saline infusions, tended to increase hippocampal LFP power at lower frequencies (<20 Hz) and to decrease power at higher frequencies (>20 Hz) although only the increase at 6–18 Hz in the burst state reached statistical significance. In contrast, there was no evidence of picrotoxin-induced power changes in the continuous LFP state. Our finding that hippocampal GABA antagonism by picrotoxin facilitates LFP oscillations at lower frequencies, including the theta range, is consistent with many previous in vitro and vivo findings indicating an inverse relationship between GABAergic inhibition and theta oscillations in the hippocampus (Colgin, 2016; Kowalczyk et al., 2013, also see Section 1). As reviewed in Section 1, some previous studies have shown that GABAergic inhibition can facilitate theta oscillations under some conditions, including when more specific manipulations of GABA transmission are used (Amilhon et al., 2015; Wulff et al., 2009) and when specific mechanisms of theta generation, such as intrinsic mechanisms (Amilhon et al., 2015), are studied separately. In our study, broadly reducing hippocampal GABA-A receptor activation by picrotoxin and not separating distinct mechanisms of theta generation, we did not find evidence for such facilitating GABA mechanisms of hippocampal theta. Although we did not find any statistically significant effects of picrotoxin on hippocampal LFP power in the beta/gamma frequencies (specifically 20–30 Hz), picrotoxin tended to decrease power in this frequency band within the burst and suppression states. These numerical decreases are consistent with previous findings that pharmacological disinhibition disrupts hippocampal in vitro gamma oscillations and that GABAergic inhibition within the hippocampus plays a key role in generating these oscillations (Bartos et al., 2007; Buzsaki & Wang, 2012; Traub et al., 2004; Whittington et al., 2000). Specifically, there is a wealth of in vitro studies showing that the GABA-A receptor antagonist bicuculline applied to hippocampal slices decreases the power of 20–30 Hz oscillations (Arai & Natsume, 2006; Boddeke, Best, & Boeijinga, 1997; Shimono, Brucher, Granger, Lynch, & Taketani, 2000; Trevino, Vivar, & Gutierrez, 2007).

4.3 | Reduced functional connectivity within the temporal to intermediate hippocampus after picrotoxin disinhibition

In the suppression and burst states, functional connectivity within the temporal to intermediate hippocampus, as reflected by phase locking of the LFP signal across the different electrodes of our recording array, was decreased in the gamma range (>20 Hz); this decrease was statistically significant in the burst state from 29.5 to 33 Hz. This is consistent with previous in vitro findings that disinhibition by morphine disrupted synchrony of gamma oscillations across a hippocampal slice preparation (Faulkner, Traub, & Whittington, 1998; Whittington, Traub, Faulkner, Jefferys, & Chettiar, 1998). Synchrony was disrupted between areas that were 1.5–2.5 mm apart, whereas effects were not observed at shorter distances (Whittington et al., 1998). It is therefore possible that, in the present study, this effect was weakened, because we assessed the collective connectivity over our 2-mm electrode array, including short distances between neighboring electrodes. Faulkner et al. (1998) also reported that a GABA-A receptor agonist applied to hippocampal slices causes a similar decrease in gamma-frequency synchrony, suggesting that such synchrony depends on a balanced level of hippocampal GABA inhibition. Furthermore, neurocomputational studies suggest that, through multiple mechanisms, GABAergic interneurons are important for the synchronization of gamma oscillations (Bartos et al., 2007; Whittington et al., 2000). For example, in a neurocomputational model of hippocampal pyramidal cells and GABAergic interneurons, blocking GABA-A receptors on the pyramidal cells abolished coherence at gamma frequencies (Traub et al., 2000). Our findings are the first in vivo findings to support these in vitro and modeling findings that the disruption of GABAergic inhibition, through blocking of hippocampal GABA-A receptors, disrupts synchronization of gamma oscillations across the hippocampus.

Finally, we found a numerical trend for picrotoxin to reduce functional connectivity in the theta frequency in the continuous hippocampal LFP state. This is consistent with previous findings that disruption of GABA-A receptor function disrupted theta coherence in vivo and in vitro (Hentschke et al., 2009; Levesque et al., 2017).

4.4 | State-dependence of enhanced multi-unit burst firing caused by hippocampal neural disinhibition

Similar to the state-dependence of LFP changes, the picrotoxin-induced enhancement of hippocampal burst firing (McGarrity et al., 2017) tended to be more pronounced in the burst and suppression states than in the continuous state, although only the analysis of burst duration revealed a statistically significant interaction of the LFP state with the infusion effect. Previous findings suggest that in an isoflurane-inducedburst-suppression state, the cortex is in a hyperexcitable state due to a decrease of excitation leading to a decrease in inhibition, which overall results in the excitation/inhibition balance being shifted toward excitation (Ferron et al., 2009). Neuronal hyperexcitability is also supported by the finding that, during the burst-suppression state, subliminal sensory stimuli activate cortical areas, including the subiculum, that are not activated by the same stimuli during other anesthetized states or the awake state (Kroeger & Amzica, 2007; Land et al., 2012). The more pronounced effects of picrotoxin during the burst and suppression states, compared to the

continuous state, may reflect neuronal hyperexcitability during these states.

4.5 | Conclusions and future directions

We have presented an objective, semi-automated method for separating three distinct hippocampal LFP states in isoflurane-anesthetized rats, including the burst, suppression, and continuous states. These states are characterized by different LFP properties and associated MUA, which are consistent with the properties of burst-suppression and "activated" or "light-anesthesia" hippocampal LFP states that have previously been identified based on visual inspection and other methods (Table 2). Furthermore, our finding that the enhanced hippocampal multi-unit burst firing induced by hippocampal picrotoxin infusion is more pronounced in the burst and suppression state, compared to the continuous state, is consistent with previous studies suggesting that the burst and suppression states are characterized by neuronal hyperexcitability (Ferron et al., 2009; Kroeger & Amzica, 2007; Land et al., 2012). Our state-separated analysis of the impact of hippocampal picrotoxin infusion on LFP properties around the infusion site revealed that, in the burst and suppression states, neural disinhibition tended to increase low-frequency oscillations (<20 Hz), including theta oscillations, and to decrease gamma frequency oscillations (>20 Hz), although only the picrotoxin-induced power increase between 6 and 18 Hz in the burst state was statistically significant. In addition, neural disinhibition reduced functional connectivity, as reflected by PLVs, across the recording area in the temporal to intermediate hippocampus at gamma frequencies in the burst state (with significant reductions compared to saline infusion between 29.5 and 33 Hz). These findings support that GABA-Areceptor-mediated mechanisms regulate hippocampal LFP oscillations in vivo (albeit under anesthesia), confirming and extending previous findings mainly from in vitro studies that GABA-Areceptor-mediated inhibition negatively modulates lower frequencies, including theta frequencies (Kowalczyk et al., 2013), and positively modulates power and connectivity at higher frequencies (Bartos et al., 2007; Buzsaki & Wang, 2012; Traub et al., 2004; Whittington et al., 2000). Similar findings albeit in neocortex have also been made in pharmacological human studies (Lozano-Soldevilla, ter Huurne, Cools, & Jensen, 2014). Cortical, including hippocampal, LFP oscillations have been suggested to be important for memory and other cognitive functions, and alterations of such oscillations have been linked to memory and other cognitive impairments (Buzsáki & Draguhn, 2004; Colgin, 2016; Uhlhaas & Singer, 2006, 2010). Consistent with this prominent view, the frequency-specific alterations of hippocampal LFP properties caused by hippocampal neural disinhibition may contribute to the memory and attentional impairments caused by the same manipulation (McGarrity et al., 2017). However, direct evidence causally linking disinhibition-induced hippocampal LFP changes to the memory and attentional deficits is lacking, and potential underlying mechanisms would also require clarification. Two important questions raised by the present findings include (a) whether similar changes in LFP oscillations would be observed without anesthesia and (b) how such changes relate to alterations in surface EEG recordings that have been reported in relevant clinical conditions, including schizophrenia and age-related cognitive decline (Hunt, Kopell, Traub, & Whittington, 2017; Uhlhaas & Singer, 2006, 2010). To address these two questions, our ongoing studies examine the simultaneous impact of hippocampal neural disinhibition on the hippocampal LFP and on surface EEG recordings in freely moving rats.

ACKNOWLEDGMENTS

This work was supported by a BBSRC iCASE PhD award in partnership with Boehringer Ingelheim to Miriam Gwilt and Tobias Bast. During preparation of this paper, Tobias Bast was a Fellow of the Research Group "Cognitive Behavior of Humans, Animals, and Machines: Situation Model Perspectives" at the Center for Interdisciplinary Research (ZiF) at Bielefeld University and benefitted from a research sabbatical granted by the School of Psychology at the University of Nottingham. Markus Bauer was supported by a Nottingham Research Fellowship by the University of Nottingham.

DATA AVAILABILITY STATEMENT

The data that support the findings of this study are available from the corresponding authors upon reasonable request.

ORCID

Miriam Gwilt https://orcid.org/0000-0003-2137-5066
Markus Bauer https://orcid.org/0000-0001-6906-1678

REFERENCES

Amilhon, B., Huh, C. Y., Manseau, F., Ducharme, G., Nichol, H., Adamantidis, A., & Williams, S. (2015). Parvalbumin interneurons of hippocampus tune population activity at theta frequency. *Neuron*, *86*(5), 1277–1289. https://doi.org/10.1016/j.neuron.2015.05.027

Arai, J., & Natsume, K. (2006). The properties of carbachol-induced beta oscillation in rat hippocampal slices. *Neuroscience Research*, *54*(2), 95–103. https://doi.org/10.1016/j.neures.2005.10.011

Aydore, S., Pantazis, D., & Leahy, R. M. (2013). A note on the phase locking value and its properties. *NeuroImage*, *74*, 231–244. https://doi.org/10.1016/j.neuroimage.2013.02.008

Bai, D., Zhu, G., Pennefather, P., Jackson, M. F., MacDonald, J. F., & Orser, B. A. (2001). Distinct functional and pharmacological properties of tonic and quantal inhibitory postsynaptic currents mediated by γ-aminobutyric acidA receptors in hippocampal neurons. *Molecular Pharmacology*, *59*(4), 814–824. https://doi.org/10.1124/mol.59.4.814

Bartos, M., Vida, I., & Jonas, P. (2007). Synaptic mechanisms of synchronized gamma oscillations in inhibitory interneuron networks. *Nature Reviews. Neuroscience*, *8*(1), 45–56. https://doi.org/10.1038/nrn2044

Bast, T., Pezze, M., & McGarrity, S. (2017). Cognitive deficits caused by prefrontal cortical and hippocampal neural disinhibition. *British Journal of Pharmacology*, *174*(19), 3211–3225. https://doi.org/10.1111/bph.13850

Bastos, A. M., & Schoffelen, J. M. (2015). A tutorial review of functional connectivity analysis methods and their interpretational pitfalls. *Frontiers in Systems Neuroscience*, *9*, 175. https://doi.org/10.3389/fnsys.2015.00175

Belluscio, M. A., Mizuseki, K., Schmidt, R., Kempter, R., & Buzsaki, G. (2012). Cross-frequencyphase-phase coupling between theta and gamma oscillations in the hippocampus. *The Journal of Neuroscience*, *32*(2), 423–435. https://doi.org/10.1523/JNEUROSCI.4122-11.2012

Benes, F. M., & Berretta, S. (2001). GABAergic interneurons: Implications for understanding schizophrenia and bipolar disorder. *Neuropsychopharmacology*, *25*(1), 1–27. https://doi.org/10.1016/S0893-133X(01)00225-1

Bieda, M. C., Su, H., & MacIver, M. B. (2009). Anesthetics discriminate between tonic and phasic gamma-aminobutyric acid receptors on hippocampal CA1 neurons. *Anesthesia and Analgesia*, *108*(2), 484–490. https://doi.org/10.1213/ane.0b013e3181904571

Boddeke, H. W., Best, R., & Boeijinga, P. H. (1997). Synchronous 20 Hz rhythmic activity in hippocampal networks induced by activation of metabotropic glutamate receptors in vitro. *Neuroscience*, *76*(3), 653–658. https://doi.org/10.1016/S0306-4522(96)00464-2

Borhegyi, Z., Varga, V., Szilagyi, N., Fabo, D., & Freund, T. F. (2004). Phase segregation of medial septal GABAergic neurons during hippocampal theta activity. *The Journal of Neuroscience*, *24*(39), 8470–8479. https://doi.org/10.1523/JNEUROSCI.1413-04.2004

Brandon, M. P., Bogaard, A. R., Libby, C. P., Connerney, M. A., Gupta, K., & Hasselmo, M. E. (2011). Reduction of theta rhythm dissociates grid cell spatial periodicity from directional tuning. *Science*, *332*(6029), 595–599. https://doi.org/10.1126/science.1201652

Buzsáki, G., & Draguhn, A. (2004). Neuronal oscillations in cortical networks. *Science*, *304*(5679), 1926–1929. https://doi.org/10.1126/science.1099745

Buzsaki, G., & Wang, X. J. (2012). Mechanisms of gamma oscillations. *Annual Review of Neuroscience*, *35*, 203–225. https://doi.org/10.1146/annurev-neuro-062111-150444

Clement, E. A., Richard, A., Thwaites, M., Ailon, J., Peters, S., & Dickson, C. T. (2008). Cyclic and sleep-like spontaneous alternations of brain state under urethane anaesthesia. *PLoS One*, *3*(4), e2004. https://doi.org/10.1371/journal.pone.0002004

Cohen, M. X. (2015). Effects of time lag and frequency matching on phase-based connectivity. *Journal of Neuroscience Methods*, *250*, 137–146. https://doi.org/10.1016/j.jneumeth.2014.09.005

Colgin, L. L. (2016). Rhythms of the hippocampal network. *Nature Reviews. Neuroscience*, *17*(4), 239–249. https://doi.org/10.1038/nrn.2016.21

Colgin, L. L., Denninger, T., Fyhn, M., Hafting, T., Bonnevie, T., Jensen, O., … Moser, E. I. (2009). Frequency of gamma oscillations routes flow of information in the hippocampus. *Nature*, *462*(7271), 353–357. https://doi.org/10.1038/nature08573

Faulkner, H. J., Traub, R. D., & Whittington, M. A. (1998). Disruption of synchronous gamma oscillations in the rat hippocampal slice: A common mechanism of anaesthetic drug action. *British Journal of Pharmacology*, *125*(3), 483–492. https://doi.org/10.1038/sj.bjp.0702113

Ferron, J. F., Kroeger, D., Chever, O., & Amzica, F. (2009). Cortical inhibition during burst suppression induced with isoflurane anesthesia. *The Journal of Neuroscience*, *29*(31), 9850–9860. https://doi.org/10.1523/JNEUROSCI.5176-08.2009

Fisahn, A., Contractor, A., Traub, R. D., Buhl, E. H., Heinemann, S. F., & McBain, C. J. (2004). Distinct roles for the kainate receptor subunits GluR5 and GluR6 in kainate-induced hippocampal gamma oscillations. *The Journal of Neuroscience*, *24*(43), 9658–9668. https://doi.org/10.1523/JNEUROSCI.2973-04.2004

Freund, T. F., & Antal, M. (1988). GABA-containing neurons in the septum control inhibitory interneurons in the hippocampus. *Nature*, *336*(6195), 170–173. https://doi.org/10.1038/336170a0

Garcia, P. S., Kolesky, S. E., & Jenkins, A. (2010). General anesthetic actions on GABAA receptors. *Current Neuropharmacology*, *8*(1), 2–9. https://doi.org/10.2174/157015910790909502

Golebiewski, H., Eckersdorf, B., & Konopacki, J. (1996). Cholinergic/GABAergic interaction in the production of EEG theta oscillations in rat hippocampal formation in vitro. *Acta Neurobiologiae Experimentalis (Wars)*, *56*(1), 147–153.

Goutagny, R., Manseau, F., Jackson, J., Danik, M., & Williams, S. (2008). In vitro activation of the medial septum-diagonal band complex generates atropine-sensitive and atropine-resistant hippocampal theta rhythm: An investigation using a complete septohippocampal preparation. *Hippocampus*, *18*(6), 531–535. https://doi.org/10.1002/hipo.20418

Hangya, B., Borhegyi, Z., Szilágyi, N., Freund, T. F., & Varga, V. (2009). GABAergic neurons of the medial septum lead the hippocampal network during theta activity. *Journal of Neuroscience*, *29*(25), 8094–8102. https://doi.org/10.1523/JNEUROSCI.5665-08.2009

Hara, K., & Harris, R. A. (2002). The anesthetic mechanism of urethane: The effects on neurotransmitter-gated ion channels. *Anesthesia & Analgesia*, *94*(2), 313–318. https://doi.org/10.1213/00000539-200202000-00015

Hayasaka, S., Phan, K. L., Liberzon, I., Worsley, K. J., & Nichols, T. E. (2004). Nonstationary cluster-size inference with random field and permutation methods. *NeuroImage*, *22*(2), 676–687. https://doi.org/10.1016/j.neuroimage.2004.01.041

Heckers, S., & Konradi, C. (2015). GABAergic mechanisms of hippocampal hyperactivity in schizophrenia. *Schizophrenia Research*, *167*(1–3), 4–11. https://doi.org/10.1016/j.schres.2014.09.041

Hentschke, H., Benkwitz, C., Banks, M. I., Perkins, M. G., Homanics, G. E., & Pearce, R. A. (2009). Altered GABAA, slow inhibition and network oscillations in mice lacking the GABAA receptor beta3 subunit. *Journal of Neurophysiology*, *102*(6), 3643–3655. https://doi.org/10.1152/jn.00651.2009

Heynen, A. J., Sainsbury, R. S., & Bilkey, D. K. (1993). Stimulation-inducedRSA-like field activity in region CA1 of the hippocampal slice: Amplitude maxima and topography. *Brain Research Bulletin*, *32*(2), 113–122.

Hunt, M. J., Kopell, N. J., Traub, R. D., & Whittington, M. A. (2017). Aberrant network activity in schizophrenia. *Trends in Neurosciences*, *40*(6), 371–382. https://doi.org/10.1016/j.tins.2017.04.003

Kay, K., & Frank, L. M. (2019). Three brain states in the hippocampus and cortex. *Hippocampus*, *29*(3), 184–238. https://doi.org/10.1002/hipo.22956

Kenny, J. D., Westover, M. B., Ching, S., Brown, E. N., & Solt, K. (2014). Propofol and sevoflurane induce distinct burst suppression patterns in rats. *Frontiers in Systems Neuroscience*, *8*, 237. https://doi.org/10.3389/fnsys.2014.00237

Koenig, J., Linder, A. N., Leutgeb, J. K., & Leutgeb, S. (2011). The spatial periodicity of grid cells is not sustained during reduced theta oscillations. *Science*, *332*(6029), 592–595. https://doi.org/10.1126/science.1201685

Konopacki, J., Gołebiewski, H., Eckersdorf, B., Błaszczyk, M., & Grabowski, R. (1997). Theta-like activity in hippocampal formation slices: The effect of strong disinhibition of GABAA and GABAB receptors. *Brain Research*, *775*(1–2), 91–98. https://doi.org/10.1016/s0006-8993(97)00919-0

Kowalczyk, T., Bocian, R., & Konopacki, J. (2013). The generation of theta rhythm in hippocampal formation maintained in vitro. *The European Journal of Neuroscience*, *37*(5), 679–699. https://doi.org/10.1111/ejn.12091

Kroeger, D., & Amzica, F. (2007). Hypersensitivity of the anesthesia-induced comatose brain. *The Journal of Neuroscience*, *27*(39), 10597–10607. https://doi.org/10.1523/JNEUROSCI.3440-07.2007

Land, R., Engler, G., Kral, A., & Engel, A. K. (2012). Auditory evoked bursts in mouse visual cortex during isoflurane anesthesia. *PLoS One*, *7*(11), e49855. https://doi.org/10.1371/journal.pone.0049855

Levesque, M., Cataldi, M., Chen, L. Y., Hamidi, S., & Avoli, M. (2017). Carbachol-induced network oscillations in an in vitro limbic system brain slice. *Neuroscience*, *348*, 153–164. https://doi.org/10.1016/j.neuroscience.2017.02.021

Lozano-Soldevilla, D., ter Huurne, N., Cools, R., & Jensen, O. (2014). GABAergic modulation of visual gamma and alpha oscillations and its consequences for working memory performance. *Current Biology*, *24*(24), 2878–2887. https://doi.org/10.1016/j.cub.2014.10.017

Lu, C. B., & Henderson, Z. (2010). Nicotine induction of theta frequency oscillations in rodent hippocampus in vitro. *Neuroscience*, *166*(1), 84–93. https://doi.org/10.1016/j.neuroscience.2009.11.072

Lustig, B., Wang, Y., & Pastalkova, E. (2016). Oscillatory patterns in hippocampus under light and deep isoflurane anesthesia closely mirror prominent brain states in awake animals. *Hippocampus*, *26*(1), 102–109. https://doi.org/10.1002/hipo.22494

Mann, E. O., Suckling, J. M., Hajos, N., Greenfield, S. A., & Paulsen, O. (2005). Perisomatic feedback inhibition underlies cholinergically induced fast network oscillations in the rat hippocampus in vitro. *Neuron*, *45*(1), 105–117. https://doi.org/10.1016/j.neuron.2004.12.016

Maris, E., & Oostenveld, R. (2007). Nonparametric statistical testing of EEG- and MEG-data. *Journal of Neuroscience Methods*, *164*(1), 177–190. https://doi.org/10.1016/j.jneumeth.2007.03.024

McGarrity, S., Mason, R., Fone, K. C., Pezze, M., & Bast, T. (2017). Hippocampal neural disinhibition causes attentional and memory deficits. *Cerebral Cortex*, *27*(9), 4447–4462. https://doi.org/10.1093/cercor/bhw247

Nava-Mesa, M. O., Jiménez-Díaz, L., Yajeya, J., & Navarro-Lopez, J. D. (2014). GABAergic neurotransmission and new strategies of neuromodulation to compensate synaptic dysfunction in early stages of Alzheimer's disease. *Frontiers in Cellular Neuroscience*, *8*, 167. https://doi.org/10.3389/fncel.2014.00167

Nolte, G., Bai, O., Wheaton, L., Mari, Z., Vorbach, S., & Hallett, M. (2004). Identifying true brain interaction from EEG data using the imaginary part of coherency. *Clinical Neurophysiology*, *115*(10), 2292–2307. https://doi.org/10.1016/j.clinph.2004.04.029

Olsen, R. W. (2006). Picrotoxin-like channel blockers of GABAA receptors. *Proceedings of the National Academy of Sciences*, *103*(16), 6081–6082. https://doi.org/10.1073/pnas.0601121103

Oostenveld, R., Fries, P., Maris, E., & Schoffelen, J. M. (2011). FieldTrip: Open source software for advanced analysis of MEG, EEG, and invasive electrophysiological data. *Computational Intelligence and Neuroscience*, *2011*, 156869–156869. https://doi.org/10.1155/2011/156869

Oostenveld, R., & Praamstra, P. (2001). The five percent electrode system for high-resolution EEG and ERP measurements. *Clinical Neurophysiology*, *112*(4), 713–719. https://doi.org/10.1016/s1388-2457(00)00527-7

Pagliardini, S., Funk, G., & Dickson, C. T. (2013). Breathing and brain state: Urethane anesthesia as a model for natural sleep. *Respiratory Physiology & Neurobiology*, *188*(3), 324–332. https://doi.org/10.1016/j.resp.2013.05.035

Pagliardini, S., Gosgnach, S., & Dickson, C. T. (2013). Spontaneous sleep-like brain state alternations and breathing characteristics in urethane anesthetized mice. *PLoS One*, *8*(7), e70411. https://doi.org/10.1371/journal.pone.0070411

Palop, J. J., & Mucke, L. (2016). Network abnormalities and interneuron dysfunction in Alzheimer disease. *Nature Reviews Neuroscience*, *17*(12), 777–792. https://doi.org/10.1038/nrn.2016.141

Patel, J., Fujisawa, S., Berenyi, A., Royer, S., & Buzsaki, G. (2012). Traveling theta waves along the entire septotemporal axis of the hippocampus. *Neuron*, *75*(3), 410–417. https://doi.org/10.1016/j.neuron.2012.07.015

Paxinos, G., & Watson, C. (1998). *A stereotaxic atlas of the rat brain*. New York, NY: Academic Press.

Penttonen, M., Kamondi, A., Acsady, L., & Buzsaki, G. (1998). Gamma frequency oscillation in the hippocampus of the rat: Intracellular analysis in vivo. *The European Journal of Neuroscience*, *10*(2), 718–728. https://doi.org/10.1046/j.1460-9568.1998.00096.x

Royer, S., Sirota, A., Patel, J., & Buzsaki, G. (2010). Distinct representations and theta dynamics in dorsal and ventral hippocampus. *The Journal of Neuroscience*, *30*(5), 1777–1787. https://doi.org/10.1523/JNEUROSCI.4681-09.2010

Shimono, K., Brucher, F., Granger, R., Lynch, G., & Taketani, M. (2000). Origins and distribution of cholinergically induced beta rhythms in hippocampal slices. *The Journal of Neuroscience*, *20*(22), 8462–8473. https://doi.org/10.1523/JNEUROSCI.20-22-08462.2000

Smythe, J. W., Colom, L. V., & Bland, B. H. (1992). The extrinsic modulation of hippocampal theta depends on the coactivation of cholinergic and GABA-ergic medial septal inputs. *Neuroscience and Biobehavioral Reviews*, *16*(3), 289–308.

Soltesz, I., & Deschenes, M. (1993). Low- and high-frequency membrane potential oscillations during theta activity in CA1 and CA3 pyramidal neurons of the rat hippocampus under ketamine-xylazine anesthesia. *Journal of Neurophysiology*, *70*(1), 97–116. https://doi.org/10.1152/jn.1993.70.1.97

Srinivasan, R., Winter, W. R., Ding, J., & Nunez, P. L. (2007). EEG and MEG coherence: Measures of functional connectivity at distinct spatial scales of neocortical dynamics. *Journal of Neuroscience Methods*, *166*(1), 41–52. https://doi.org/10.1016/j.jneumeth.2007.06.026

Stanley, E. M., Fadel, J. R., & Mott, D. D. (2012). Interneuron loss reduces dendritic inhibition and GABA release in hippocampus of aged rats. *Neurobiology of Aging*, *33*(2), 431. e431–431. e413. https://doi.org/10.1016/j.neurobiolaging.2010.12.014

Steriade, M., Amzica, F., & Contreras, D. (1994). Cortical and thalamic cellular correlates of electroencephalographic burst-suppression. *Electroencephalography and Clinical Neurophysiology*, *90*(1), 1–16.

Thomé, A., Gray, D. T., Erickson, C. A., Lipa, P., & Barnes, C. A. (2016). Memory impairment in aged primates is associated with region-specific network dysfunction. *Molecular Psychiatry*, *21*(9), 1257–1262. https://doi.org/10.1038/mp.2015.160

Tiesinga, P. H., Fellous, J. M., José, J. V., & Sejnowski, T. J. (2001). Computational model of carbachol-induced delta, theta, and gamma oscillations in the hippocampus. *Hippocampus*, *11*(3), 251–274. https://doi.org/10.1002/hipo.1041

Tóth, K., Freund, T., & Miles, R. (1997). Disinhibition of rat hippocampal pyramidal cells by GABAergic afferents from the septum. *The Journal of Physiology*, *500*(2), 463–474. https://doi.org/10.1113/jphysiol.1997.sp022033

Traub, R. D., Bibbig, A., Fisahn, A., LeBeau, F. E., Whittington, M. A., & Buhl, E. H. (2000). A model of gamma-frequency network oscillations induced in the rat CA3 region by carbachol in vitro. *The European Journal of Neuroscience*, *12*(11), 4093–4106.

Traub, R. D., Bibbig, A., LeBeau, F. E., Buhl, E. H., & Whittington, M. A. (2004). Cellular mechanisms of neuronal population oscillations in the hippocampus in vitro. *Annual Review of Neuroscience*, *27*, 247–278. https://doi.org/10.1146/annurev.neuro.27.070203.144303

Trevino, M., Vivar, C., & Gutierrez, R. (2007). Beta/gamma oscillatory activity in the CA3 hippocampal area is depressed by aberrant GABAergic transmission from the dentate gyrus after seizures. *The Journal of Neuroscience*, *27*(1), 251–259. https://doi.org/10.1523/JNEUROSCI.3815-06.2007

Tukker, J. J., Fuentealba, P., Hartwich, K., Somogyi, P., & Klausberger, T. (2007). Cell type-specific tuning of hippocampal interneuron firing during gamma oscillations in vivo. *The Journal of Neuroscience*, *27*(31), 8184–8189. https://doi.org/10.1523/JNEUROSCI.1685-07.2007

Uhlhaas, P. J., & Singer, W. (2006). Neural synchrony in brain disorders: Relevance for cognitive dysfunctions and pathophysiology. *Neuron*, *52*(1), 155–168. https://doi.org/10.1016/j.neuron.2006.09.020

Uhlhaas, P. J., & Singer, W. (2010). Abnormal neural oscillations and synchrony in schizophrenia. *Nature Reviews Neuroscience*, *11*(2), 100–113. https://doi.org/10.1038/nrn2774

Whittington, M. A., Traub, R. D., Faulkner, H. J., Jefferys, J. G., & Chettiar, K. (1998). Morphine disrupts long-range synchrony of gamma oscillations in hippocampal slices. *Proceedings of the National Academy of Sciences of the United States of America*, *95*(10), 5807–5811.

Whittington, M. A., Traub, R. D., Kopell, N., Ermentrout, B., & Buhl, E. H. (2000). Inhibition-based rhythms: Experimental and mathematical observations on network dynamics. *International Journal of*

Psychophysiology, *38*(3), 315–336. https://doi.org/10.1016/s0167-8760(00)00173-2

Wolansky, T., Clement, E. A., Peters, S. R., Palczak, M. A., & Dickson, C. T. (2006). Hippocampal slow oscillation: A novel EEG state and its coordination with ongoing neocortical activity. *The Journal of Neuroscience*, *26*(23), 6213–6229. https://doi.org/10.1523/JNEUROSCI.5594-05.2006

Wulff, P., Ponomarenko, A. A., Bartos, M., Korotkova, T. M., Fuchs, E. C., Bahner, F., … Monyer, H. (2009). Hippocampal theta rhythm and its coupling with gamma oscillations require fast inhibition onto parvalbumin-positive interneurons. *Proceedings of the National Academy of Sciences of the United States of America*, *106*(9), 3561–3566. https://doi.org/10.1073/pnas.0813176106

Ylinen, A., Bragin, A., Nádasdy, Z., Jandó, G., Szabo, I., Sik, A., & Buzsáki, G. (1995). Sharp wave-associatedhigh-frequency oscillation (200 Hz) in the intact hippocampus: Network and intracellular mechanisms. *Journal of Neuroscience*, *15*(1), 30–46. https://doi.org/10.1523/JNEUROSCI.15-01-00030.1995

How to cite this article: Gwilt M, Bauer M, Bast T. Frequency- and state-dependent effects of hippocampal neural disinhibition on hippocampal local field potential oscillations in anesthetized rats. *Hippocampus*. 2020;1–23. https://doi.org/10.1002/hipo.23212